Evolution & Development

WILEY

RESEARCH ARTICLE

Transient Epithelial Mimicry by Neural Crest Mesenchyme Anchors Cell Condensations Across Avian Beaks

Carmen Sánchez Moreno[1,2] | Alexander V. Badyaev[1,3]

[1]Department of Ecology & Evolutionary Biology, University of Arizona, Tucson, Arizona, USA | [2]Department of Molecular and Cellular Biology, University of Arizona, Tucson, Arizona, USA | [3]BIO5 Institute, University of Arizona, Tucson, Arizona, USA

Correspondence: Alexander V. Badyaev (abadyaev@arizona.edu)

Received: 11 August 2025 | **Revised:** 9 March 2026 | **Accepted:** 8 May 2026

Funding: National Science Foundation, Grant/Award Numbers: IBN-0218313, DEB-1754465

Keywords: beak morphogenesis | cell condensations | developmental plasticity | epithelial–mesenchymal signaling | house finch | neural crest cells | passerine bird | positional effects | stem cells

ABSTRACT

Multicellular morphogenesis must balance organismal cohesion with local tissue differentiation. In avian beaks, conserved epithelial–mesenchymal crosstalk underlies the formation of condensations of migratory neural crest mesenchymal (NCM) cells, yet how these cells acquire precise positional information without compromising stemness is unclear. Using high-throughput quantification of protein expression and morphology of 2.1 million cells and 16 stereotypical condensations across upper and lower beaks, we resolve the temporal sequence of condensation anchoring. We find that a subset of mesenchymal cells at each condensation site transiently matches protein expression in the overlying epithelium, which diverges as development proceeds. Propagation of these location-specific expression profiles into mesenchyme establishes signaling boundaries that anchor forming condensations. As NCM cells accumulate within these boundaries, they progressively erase location-specific protein profiles and restore their region- and tissue-specific protein expression. These transient location-matching and cell-homogenization phases show how migrating NCM cells achieve precise positional anchoring while retaining stemness needed for regional specifications. Ultimately, spatiotemporal modulations of a conserved regulatory network by predictable patterns of cell proliferation and migration can underpin the remarkable evolutionary diversification of avian beaks.

1 | Introduction

In multicellular development, cell differentiation occurs largely in the context of cell groups, where cell contacts synchronize and channel their variability and prime fate transitions (Akieda et al. 2019; Atchley and Hall 1991; Dunlop and Hall 1995; B. K. Hall 1978, 2003; Soldatov et al. 2019; Tacchetti et al. 1992). Yet how uniform cells aggregate and what guides the spatial and temporal distribution of the resulting cell condensations remain poorly understood. Crucially, it is unclear whether these two aspects are linked: condensations are often viewed as an emergent outcome of aggregation and adhesion of individual cells (Barna and Niswander 2007; Cottrill et al. 1987; Glimm et al. 2014; Kaul et al. 2015; Svandova et al. 2020; Widelitz et al. 1993), yet their highly stereotypical distribution implies specific positional sensitivity (Abramyan and Richman 2015; Hu et al. 2015; Wu et al. 2006). This combination of universality and specificity is particularly striking for distantly induced multipotent cells that travel through diverse signaling environments before arriving at local contexts where they form region-appropriate aggregations (Buitrago-Delgado et al. 2015; Gitton et al. 2010; B. K. Hall 1980, 2018; Hovland et al. 2022; Kaucka et al. 2016; Paudel et al. 2022; Woronowicz and Schneider 2019). Mechanisms that modulate the spatial and

Summary

- Transient adoption of epithelial signaling can reconcile stemness and regional specification in neural crest cell condensations.
- This developmental organization balances global coordination and local specialization and can facilitate evolutionary diversification of avian beaks.

temporal sensitivity of these cells and reconcile their stemness with their ability to organize locally appropriate tissues are central to the evolution of morphological diversity.

A particularly well-studied example is craniofacial morphogenesis in vertebrates, where migrating neural crest-derived mesenchymal (NCM) cells that build the upper and lower jaws combine remarkable regulatory autonomy with an equally striking ability to orchestrate region-specific molecular and cellular interactions (Creuzet et al. 2005; Fonseca et al. 2017; B. K. Hall 1999; Hu et al. 2015; Jheon and Schneider 2009; Minoux and Rijli 2010; Santagati and Rijli 2003; Schneider 2024; Schneider and Helms 2003; Selleri and Rijli 2023; Welsh and O'Brien 2009). This combination has fueled a long-standing research program addressing whether spatiotemporal specificities are embedded in NCM cells at the time and place of their induction, accumulate in NCM cell groups during migration, or emerge through cellular and molecular interactions with local tissues (B. K. Hall 1999; Minoux and Rijli 2010; Schneider 2018; Selleri and Rijli 2023). Classical grafting experiments, particularly in birds, found evidence for all of these processes (Creuzet et al. 2005; J. Hall et al. 2014; Hu and Marcucio 2012; Hu et al. 2003; Noden 1983; Ray and Chapman 2015; Richman and Tickle 1989; Trainor et al. 2002). Essentially, NCM cells, although retaining molecular memory of their origin and accumulating migration bias en route still retain enough multipotency upon their arrival to orchestrate region-specific condensations (Buitrago-Delgado et al. 2015; Dupin et al. 2018; Kelsh et al. 2021). Yet, the epithelial–mesenchymal signaling essential for proper placement of condensations is deeply evolutionarily conserved (Eames and Helms 2004; Le Douarin et al. 2004; Lu et al. 2024), which raises the question of how placement specificity emerges.

Mechanisms capitalizing on predictable material properties of cells and tissues (such as tension or elasticity), as well as on measures of distance and time are particularly suited for positional regulation, including in NCM tissues (Badyaev et al. 2025; Barriga et al. 2018; Francis-West et al. 1998; Lenne et al. 2021; Medeiros and Crump 2012; Meinecke et al. 2018; Ransom et al. 2018). One potential resolution therefore is that the distribution of condensations might be linked to the distance and timing of NCM cell's migration and to associated changes in either sensitivity to epithelial signaling or epithelial signaling itself caused by growth expansion. Indeed, the ability of epithelial signaling to initiate mesenchymal condensation is time-sensitive, NCM cell fate specification is affected by the accumulating effects of migration, and expanding epithelium produces a feed-forward signaling gradient (Celá et al. 2016; Haworth et al. 2004; Liu et al. 2005; MacDonald and Hall 2001; Merrill et al. 2008; Welsh and O'Brien 2009). Thus, it is important to establish the time, place, and context in which NCM cells first acquire location specificity and to identify how time- and distance-dependent local divergence modulates deeply conserved epithelial–mesenchymal signaling.

Here, we take this approach by tracing the temporal onset of regional specificity in cellular and molecular determinants of NCM condensations across the beak primordia of the house finch (*Haemorhous mexicanus*). We specifically focus on the role of the boundary that delineates condensations within the fields of mesenchymal cells and is essential for condensation growth, modulation of external inputs, maintenance of uniformity, and ultimate differentiation (Giffin et al. 2019; B. K. Hall and Miyake 2000; He et al. 2025). Whether the boundary is a cause or consequence of condensation formation is unclear; it can emerge as a consequence of cell aggregation and resulting radial signaling gradient, or it can precede condensations through upregulation of signaling in mesenchymal cells in interaction with extracellular matrix components, producing physical or signaling barriers facilitating sorting and retention of migrating NCM cells (Giffin et al. 2019; B. K. Hall and Miyake 2000; Widelitz et al. 1993). Here, we explore these roles with particular focus on the onset of location specificity in condensation anchoring (e.g., Figure 1f); we specifically test whether NCM cells propagate epithelial signaling into the mesenchyme by capitalizing on cell growth, rearrangement, and material transitions (Badyaev et al. 2025; Conigliaro and Cicchini 2019; Kicheva and Briscoe 2023; Kornberg and Roy 2014; Wood et al. 2021).

We first establish the temporal sequence of tissues reorganization involved in condensation formation (Figures 1 and S2) and the contribution of cellular and molecular mechanisms to this reorganization (Figure 2). We then capitalize on extensive developmental divergence and tissue reorganization within and between the upper and lower jaw primordia (Depew and Compagnucci 2008; Gitton et al. 2010; Tak et al. 2017) to statistically partition variance associated with the global, regional, and locally unique molecular and cellular processes during condensation formation (Figures 1 and 3).

Using an analytical approach that allows tracing millions of cells throughout development across the upper and lower beak primordia (Table 1 and Figure S1), we find that condensations are preceded by the formation of signaling boundaries—a subset of NCM cells extending locally unique protein profiles of overlying epithelium into the mesenchyme, followed by the accumulation and compaction of NCM cells within these boundaries and subsequent cellular and molecular homogenization. We suggest that these phases of transient specialization and homogenization in migratory NCM cells can reconcile their undiminished developmental potential with location-specific anchoring of condensations. Such developmental organization allows for the spatiotemporal modulation and recombination of conserved regulatory modules, facilitating evolutionary diversification of avian beaks.

2 | Materials and Methods

2.1 | Data Collection and Sample Sizes

We measured cell morphology and protein expression in upper and lower beak primordia of house finch embryos across

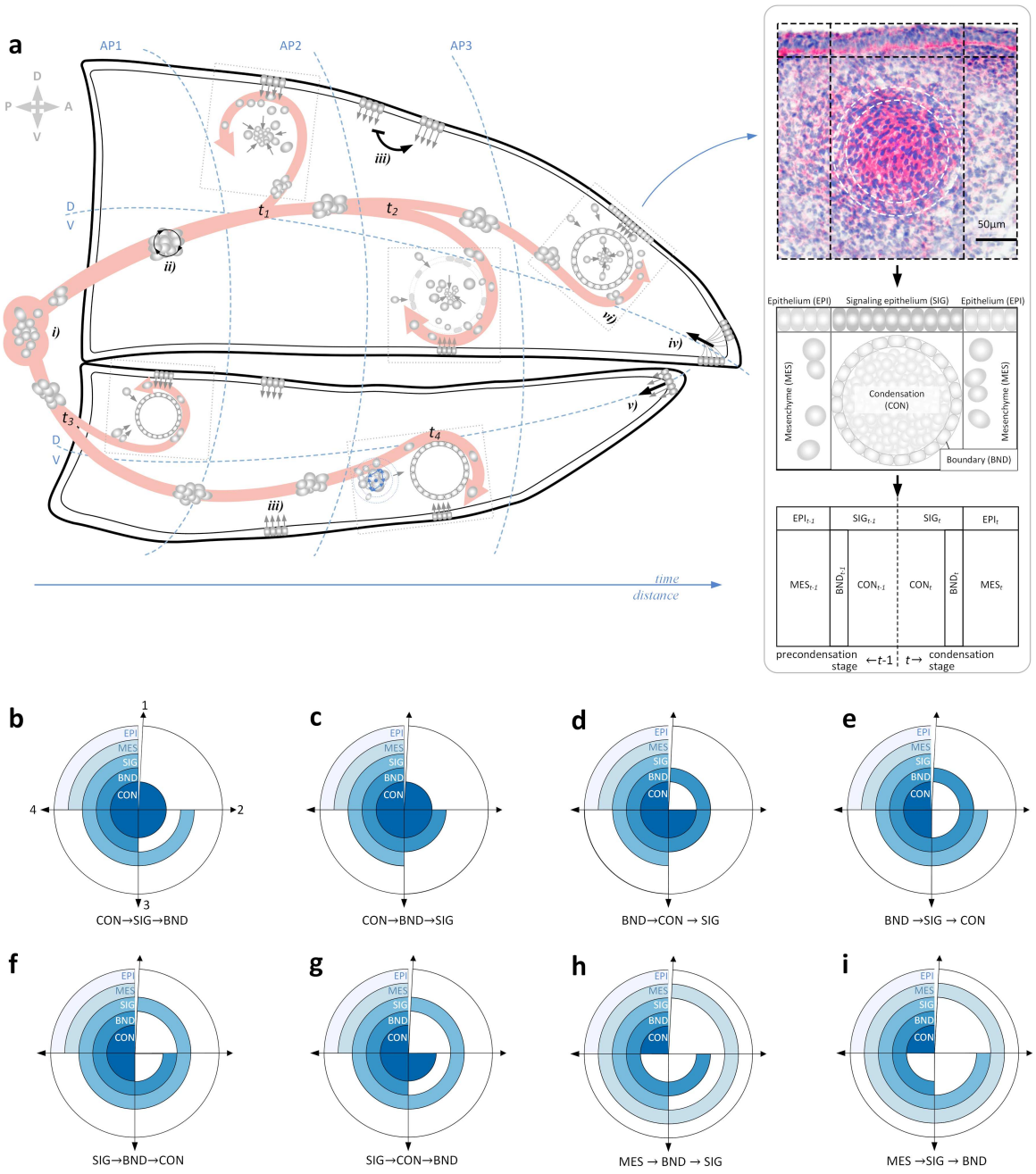

FIGURE 1 | Temporal sequence of condensation origin. (a) Schematics of NCM cell migration streams (coral arrows) from their induction sites in neural folds (*i*) to the future condensations distributed across anterior–posterior (AP) and dorsoventral (DV) zones of the upper and lower beaks. En route, groups of migrating NCM cells interact with each other (*ii*), experience external input, such as unfolding epithelial signaling (*iii*), and axial signaling gradients emanating from the base and tip of beaks (*iv* and *v*). Dashed rectangles at condensation sites represent grid boxes analyzed in this study (see Section 2). Insert (*vi*) shows an example of Ihh expression (magenta) in studied tissues (see also Figure S2) and corresponding tissue classification within each grid box: CON—condensation, BND—boundary, MES—uncondensed mesenchyme, SIG—signaling epithelium overlying condensation, and EPI—adjacent epithelium. Also shown is the corresponding tissue scheme for reporting results for pre- $(t-1)$ and condensation (t) stages. (b and i) Known and proposed temporal sequences of condensation origin. Arriving NCM cells either induce local epithelium signaling (b) or proliferate, forming condensation and its boundary, subsequently inducing epithelial signaling (c); compaction of earlier arriving NCM cells forms a boundary that sorts or traps cells either producing condensations directly (d) or inducing epithelial signaling which then maintains condensation formation (e), signaling epithelium either induces the formation of a boundary leading to accumulation of arriving NCM cells (f) or attracts migrating cells causing them to aggregate and form the condensation directly (g). Dynamically interacting NCM cells acquire rigidity and either form a boundary (h) or express proteins enabling them to induce or respond to local epithelial signaling (i). [Color figure can be viewed at wileyonlinelibrary.com]

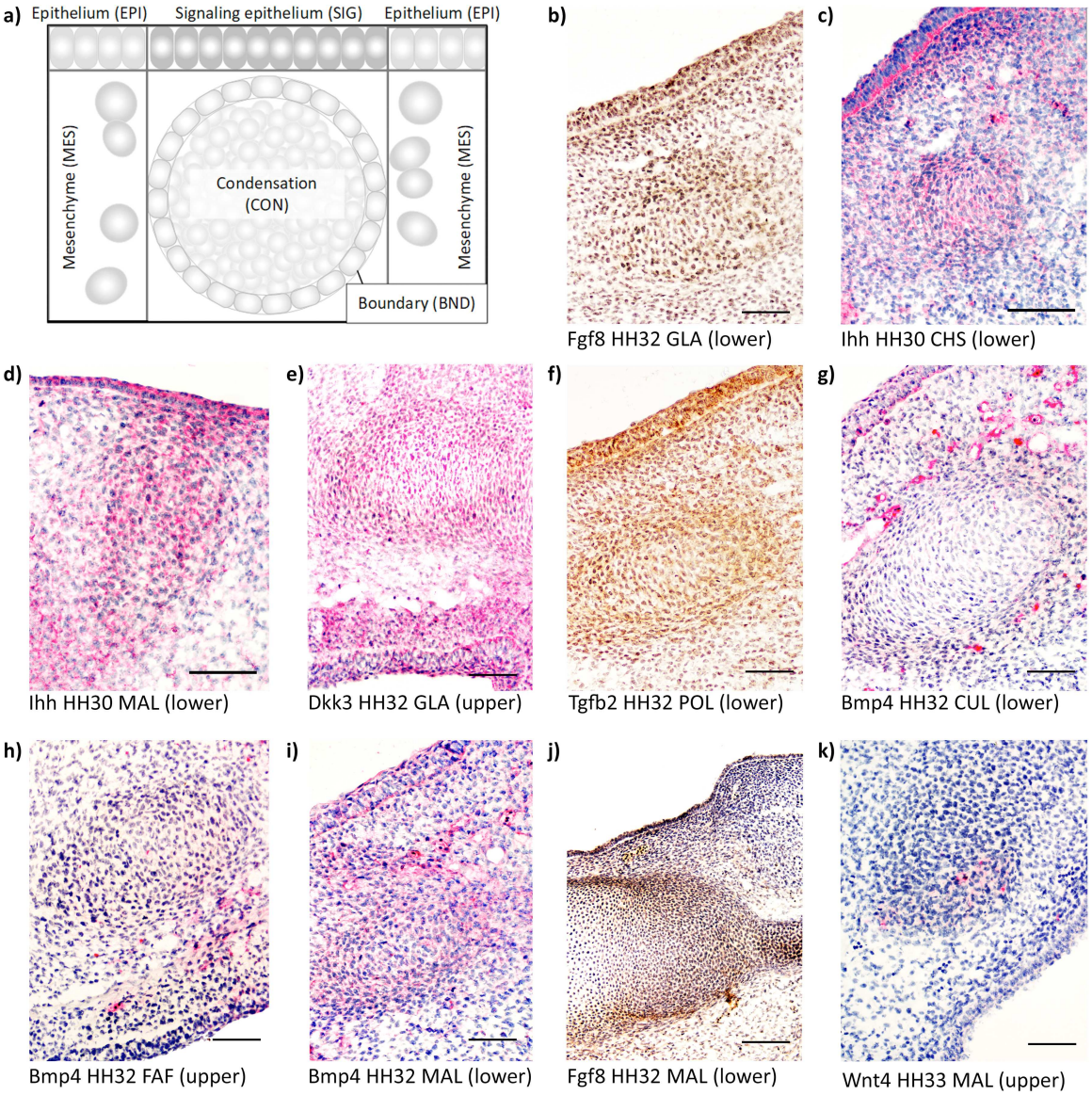

FIGURE 2 | Representative examples of histological grid boxes ($n = 35{,}755$; Table 1 and Figure S1) showing mesenchymal cell condensations and overlying epithelium (panel (a) shows the scheme from Figure 1). Text under panels (b–k) shows protein expression, developmental stage, population abbreviation, and jaw. Scale bar is 50 μm. [Color figure can be viewed at wileyonlinelibrary.com]

developmental stages HH25-36 from five genetically distinct population groups (Table S1, Badyaev 2010; Potticary et al. 2020). Protocols for egg collection, incubation to the required developmental stage, calibrated with zebra finch developmental staging (Murray et al. 2013), and field storage of samples are in Badyaev et al. (2025). Beaks were cryosectioned at 8 μm and stored at −80°C. Thirteen sections per individual were obtained at beak midline: one section was stained with Alcian blue hematoxylin and eosin (H&E; U. Rochester MC) to delineate the area of interest (AOI) and tissues, 12 were used in immunohistochemical (IHC) analysis of 8 proteins described below.

2.2 | Tissue Assignment, Condensation Identification, and Cell Morphology

Cell measurements and protein expression data were collected within AOI of the upper and lower beak that was delineated by landmarks homologous across developmental stages and confirmed with H&E histological staining (C. A. Lee et al. 2024). Briefly, the upper beak AOI was from the point of inflection of the upper beak, to the lower outer tissue of the brain/eye to the inner edge of the mouth, just past the palatine process, but not including the palatine process, to the tip of the beak, along the inner edge of the egg tooth and back to the point of upper beak inflection. The lower beak AOI was from the tip of the lower beak, down the inner edge past the developing tongue until the beak begins to widen, across the lower beak, and back to the lower beak tip along the outer edge. Four equal anterior–posterior (AP) and two equal dorsoventral (DV) zones were established within the upper and lower beaks based on the uniform size of overlaying grid (Figure 1a).

In this work, we focused only on precondensation ($t-1$) and the earliest condensation (t) stages (Figure 3a), excluding any condensations that initiated tissue differentiation because it is

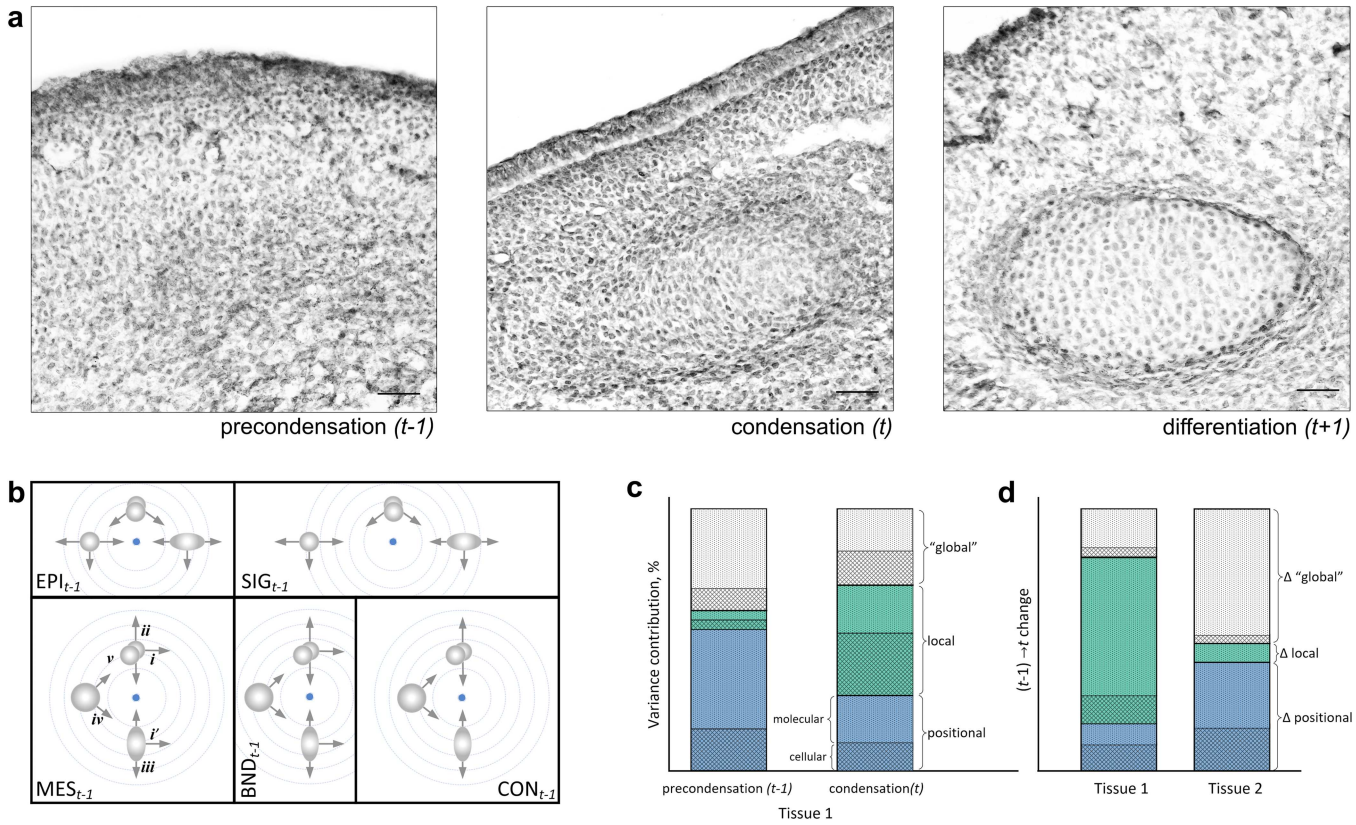

FIGURE 3 | Cellular and molecular processes of condensation origin and statistical inference into their location specificity. (a) Stages of condensation formation and differentiation within a grid box (Figure 1a inset) used in the workflow (Figure S1). (b) Comparison of cell morphology and protein expression in each tissue at stages across scenarios of Figure 1. (b-i) informs how epithelial–mesenchymal interactions can orchestrate location-specific condensations. Cells can show polarity toward the sites of future condensations (*i*; *i′*- shows variation in cell polarity), toward (*ii*) or away (*iii*) from epithelial or mesenchymal cells, forming cell groups (*iv*). These movements along with changes in cell density and proliferation (*v*) can transport, dilute, or delimit spread of molecular signaling (dashed circles) leading to compartmentalization of condensation sites. Tissue abbreviations as in Figure 1. (c, d) Statistical variance partitioning in molecular and cellular mechanisms to infer sources of variance during condensation formation. Predictions illustrating an approach to distinguish "local" context-dependent variance (contribution of interaction terms between condensation placements along AP and DV axes and between jaws), "positional" gradient-based variance (contribution of condensation placement along AP and DV axes or in different jaws), and "global" variance unexplained by any location- or jaw-based measure, either directly or in interaction, and likely representing tissue-specific variation or unmeasured effects (see Section 2). Hypothetical contributions of molecular and cellular mechanisms are shown. (c) Variance partitioning between pre- ($t-1$) and condensation (t) stages. (d) Change between stages for two tissues. Tissue 1 shows *an increase in local specificity*, especially of molecular contributors, such as those associated with greater developmental specification, and *lessening contribution of positional gradients* in cellular and molecular effects. Tissue 2 shows *diminishing local specificity*, expected under tissue reprogramming in which positional gradients no longer explain significant variance. *Increased contribution of positional gradients* reflects tissue reorganization, here also implying interdependence of condensations due to their temporal synchrony or juxtaposition. [Color figure can be viewed at wileyonlinelibrary.com]

associated with distinct expression of studied proteins (Celá et al. 2016; Duckworth et al. 2025; Ray and Chapman 2015). The workflow for tissue assignment and curation, and high-throughput measurements of cell morphology, variability and density, and protein expression using software we developed for this work (C. A. Lee et al. 2024) is detailed in Figure S1. We focused on 16 stereotypical mesenchymal condensations (8 in upper beak and 8 in lower) that were repeatably identifiable in > 80% of samples (Tables 1, S2 and Figures S1–S3). In the upper beak, three of these condensations (U2, U5, and U8) were parts of the frontonasal facial prominence, three others (U4, U10, and U12) were contained within the lateral nasal facial prominence and two (U6–7 and U9) eventually merge into the maxillary prominence. In the lower beak, six condensations will form the basihyal (L3–6) and paraglossal (L1, L5, L7) cartilages and associated muscle (L8 and L9). L2 will form the dentary bone and L4 –Meckel's cartilage (Tables 1 and S2). Within each grid box, for all cells, we measured area (μm^2), perimeter (μm), aspect ratio (AR) $= \frac{a}{b}$ (major and minor axis of the best fitting ellipsoid), solidity, circularity, the cell shape index $\bar{p}_o = \frac{Perimeter}{\sqrt{Area}}$, and polarity angle of the major axis (folded into 0°–180° range). For each grid box (~ 130 cells per box, $n = 2{,}120{,}160$ cells total), we also calculated the mean and standard deviation for these measures.

2.3 | Immunohistochemistry

We measured the expression of eight proteins that play a central role in avian beak development (Abzhanov et al. 2004, 2006;

TABLE 1 | Sample sizes for condensation-containing grid boxes ($n_{boxes} = 35{,}755$; $n_{cells} = 2.12 \times 10^6$) across tissue types during (t) and prior ($t-1$) to condensation formation across tissue types, beak prominences, future tissue types (F_Tissue), and upper and lower beak (Jaw).

				Condensation tissues (t)					Tissues prior to condensation formation ($t-1$)				
Jaw	**Prominence**	**F_Tissue**	**Condens**	**BND_t**	**CON_t**	**EPI_t**	**MES_t**	**SIG_t**	**BND_{t-1}**	**CON_{t-1}**	**EPI_{t-1}**	**MES_{t-1}**	**SIG_{t-1}**
Upper	Frontonasal	Cartilage	U2	204	250	540	435	125	12	13	25	54	14
		Cartilage	U5	274	220	371	606	24	20	33	20	91	17
		Muscle	U8	276	85	462	397	28	68	85	90	238	17
	Lateral nasal	Cartilage	U4	384	452	333	608	38	31	84	20	153	1
		Cartilage	U10	81	108	99	288	1	25	50	27	134	23
		Cartilage	U12	234	185	260	429	12	26	73	38	131	17
	Maxillary	Cartilage	U6,7	274	334	688	1060	17	93	330	165	495	81
		Muscle	U9	112	38	677	447	40	36	53	78	155	39
Lower	Mandibular	Cartilage	L1	531	221	625	661	34	7	30	21	42	10
		Cartilage	L3,6	518	187	1257	488	77	191	161	289	308	90
		Cartilage	L5	294	33	679	590	0	55	94	83	306	15
		Cartilage	L7	504	201	645	449	21	44	39	72	125	14
		Muscle	L8	824	253	824	1156	26	107	102	122	250	35
		Muscle	L9	301	26	657	654	18	96	126	60	252	18
		Bone	L2	532	219	627	670	12	9	38	22	43	7
	Meckel's	Cartilage	L4	467	121	1344	818	8	27	56	57	104	5

Badyaev et al. 2026; Fritz et al. 2014; Mallarino et al. 2011, 2012; Ray and Chapman 2015; Wu et al. 2004, 2006): β-catenin, bone morphogenic protein 4 (Bmp4), calmodulin1 (Calm1), dickkopf homolog 3 (Dkk3), fibroblast growth factor 8 (Fgf8), Indian hedgehog (Ihh), transforming growth factor beta 2 (TGFβ2), and wingless type 4 (Wnt4). For immunostaining, we used anti-β-catenin (610153, 1:16,000, BD Transduction Laboratories), anti-CaM (sc-137079, 1:15, Santa Cruz Biotechnology), anti-Wnt4 (ab91226, 1:800; Abcam), anti-Tgfβ2 (ab36495, 1:800, Abcam), anti-Bmp4 (ab118867, 1:100, Abcam), anti-Ihh (ab184624, 1:100, Abcam), anti-Dkk3 (ab214360, 1:100, Abcam), and anti-Fgf8 (89550, 1:50, Abcam) antibodies using methods described previously (C. A. Lee et al. 2024). Validations confirming the specificity of stains are in Badyaev et al. (2025). Reactions were visualized with either diaminobenzidine (DAB, Elite ABC HRP Kit, PK-6100, Vector Labs) or Vector Red Alkaline Phosphatase substrate and Vectastain ABC-AP Kit (AK-5000, Vector Labs) and nuclei were counterstained with hematoxylin. Three slides, each containing four tissue sections (12 sections per embryo) were run with the following grouped antibodies: (i) β-catenin, Fgf8, Tgfβ2 and no primary control, (ii) Bmp4, Wnt4, Ihh and no primary control, and (iii) Dkk3 and no primary control, and CaM and no primary control. These were imaged and named according to embryo ID, protein, developmental stage, and IHC run to enable high-throughput processing of cell-based expression as described in C. A. Lee et al. (2024). Protein expression was measured as the ratio of cells expressing the protein to the total number of cells within the tissue. Across IHC runs, we randomized the assignment of sections from different populations and stages.

2.4 | Statistical Analyses

To achieve normal distribution, reduce skewness and stabilize variance, we used the Box–Cox transformation with $\lambda = 0.5$ for raw values of protein expression, the standard logarithm transformation for cell morphology measures and the arcsine transformation for cell density and AR proportional measures. We derived linear principal components of the normalized and standardized measurements of cell morphology and variability that reduced these measurements to two dimensions—cell shape, cell size as well as variation in these two parameters (Table S3). We used a mixed-effects model of Proc Mixed (SAS 9.4), to compute the least squares (LS) means of cell morphology and protein expression across tissues, time periods, and condensation placements, and compared them after a Sidak adjustment for multiple comparisons. Population and embryo identity were treated as random effects. To evaluate tissue divergence and its change between time periods, we computed pairwise Euclidean distances between the tissues in molecular (8 factors) and cellular (5 factors) divergence. We compared cell polarity angles with Watson–Williams axial test and adjusted multiple pairwise tissue comparisons with Bonferroni correction.

In addition to the strong positional effects of placement along AP and DV axes across jaws or tissues, the majority of cellular and molecular mechanisms also showed substantial context-dependency as evidenced by significant two- and three-way interactions among these predictors. This gave us an opportunity to directly compare the contribution of positional effects (zones along AP and DV axes and jaw placement, Figure 1a), local, or region-specific "local" effects (interactions between these predictors) and of effects not accounted for by either gradient or local placement (which includes tissue specificity of cellular and molecular mechanisms; Figure 3). For every tissue type, we compared the explanatory power of context-specific ("local") effects in cellular and molecular responses by contrasting the marginal R^2 from a full model—which included all predictors and a full array of their interactions—with that of a reduced model which excluded all interaction terms. Both models were estimated using maximum likelihood approach in mixed-effects models, in which fixed effects captured the primary predictors with Proc PLM (SAS 9.4). Fixed-effect predictions were generated and their variance computed, while random and residual variances were extracted from the covariance parameters. We calculated the marginal R^2 as the ratio of the variance due to fixed effects to the total variance (the sum of fixed, random, and residual variances). Contribution of the context-specific "local" predictors was the difference of marginal R^2s between the full and reduced models, contribution of positional effects was contribution of fixed positional (noninteraction positional predictors, i.e., zones and jaws) to the full model, and global "unexplained" variance was calculated as the variance in cellular or regulatory effect, not explained by the model (Figure 3c,d).

3 | Results

3.1 | Matching Protein Profiles of Overlying Epithelium Precedes Condensation Formation

Although not yet morphologically distinct from surrounding mesenchyme, future boundary cells had elevated Ihh compared to all other tissues, and also had distinct expression of β-catenin, Bmp4, Dkk3, and Tgfβ2 relative to adjacent mesenchyme, as well as different Fgf8 and β-catenin expression compared to the overlying epithelium (Figure 4a and Tables 2, S4). Protein profiles of future boundary cells were more similar to the overlying epithelium than to any other tissue, including the adjacent mesenchyme of future condensations (Figure 5a,e). Future condensation cells expressed lower β-catenin compared to both the overlying epithelium and the future boundaries but did not differ in expression of other proteins or cell morphology from the surrounding mesenchyme (Figure 4 and Table S4). Prior to condensation formation, the epithelium overlying future condensations was similar to the adjacent epithelium in protein expression and cell morphology (Figure 5). Outside of future condensation sites, mesenchymal tissues showed polarity toward the sites of future condensations whereas future boundary cells showed strong polarity toward the overlying epithelium (Figure 6a). Mesenchymal and epithelial tissues differed in both protein profiles (except for Ihh and CaM) and cell morphology and variability (Figures 4, 6 and Tables 2, S4).

3.2 | Enclosed Condensations Rapidly Diverge From Adjacent Tissues

Enclosed condensations contained smaller, more densely packed, and more uniform cells compared to the surrounding

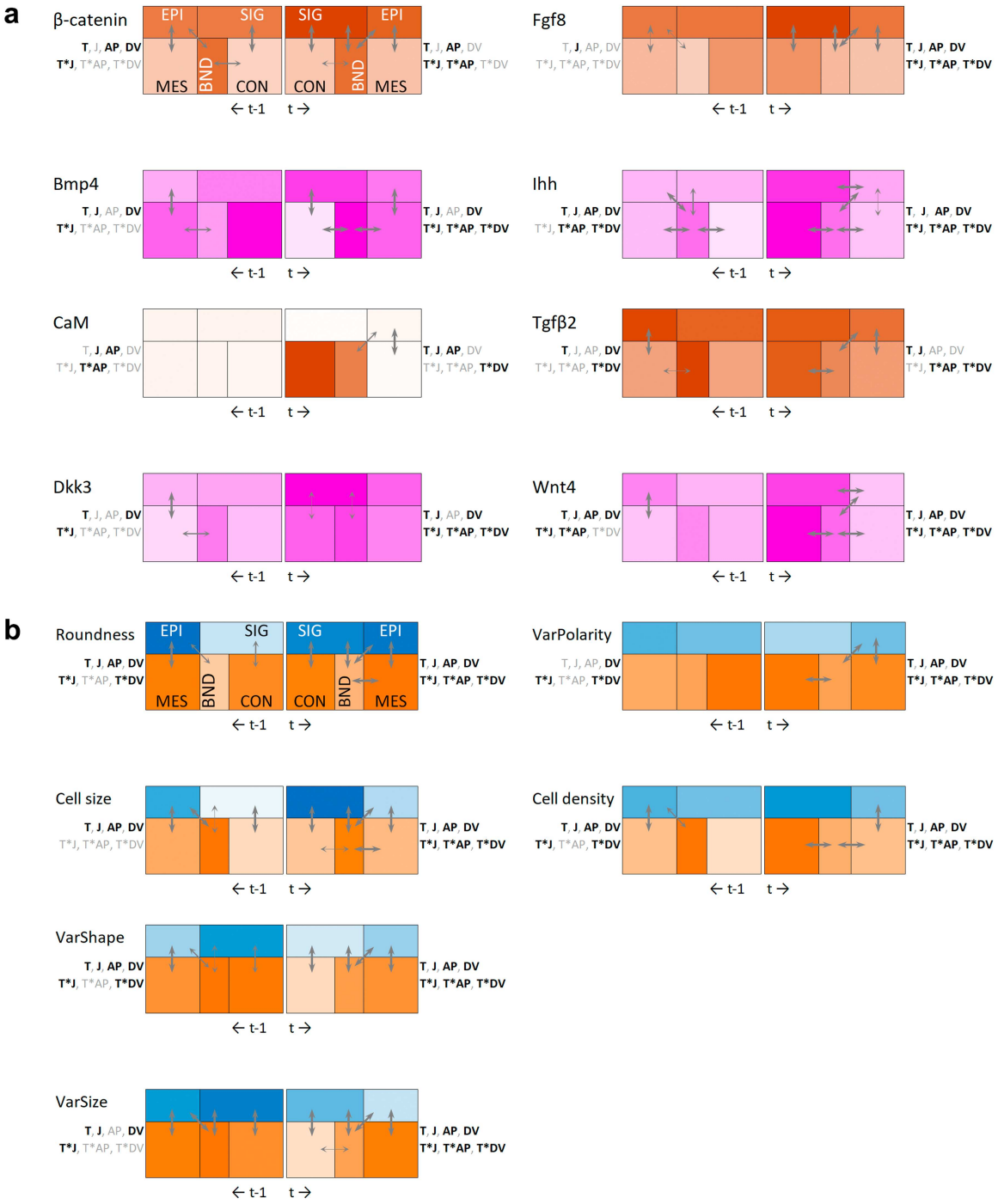

FIGURE 4 | Tissue-specific (a) protein expression and (b) cell morphology during pre- ($t-1$, left side) and condensation (t, right side) stages. Schematics of tissues follow insert of Figure 1a. Shown are LS means and significant differences between them (based on Tables 2 and S4) as well as associated dependency on tissue type (T), jaw (J), anterior–posterior (AP) or dorsoventral (DV) zones, as well as on interaction between the tissue type and jaw (T*J), anterior–posterior (T*AP) or dorsoventral (T*DV) axes (based on Table 2). Bold values indicate significance after adjustment for multiple pairwise comparisons. Arrows indicating the LS mean differences are proportional to adjusted p value (thin arrows: $p \leq 0.1$, medium: $0.05 \leq p < 0.1$, and thick arrows: $p < 0.01$, based on Table S3). Color saturation is proportional to values for all tissues and time periods; color scheme reflects IHC staining group in (a) and is separate for mesenchymal (MES, BND, CON) and epithelium (EPI, SIG) tissues in (b). [Color figure can be viewed at wileyonlinelibrary.com]

boundary, and expressed lower β-catenin and Bmp4, but higher Ihh, Wnt4, and Tgfβ2 (Figures 4a,b, 5b,d, 6b and Table S4). Condensed and uncondensed mesenchyme differed in the expression of Bmp4, Fgf8, Ihh, Tgfβ2, and Wnt4; condensations contained cells that were more uniform in size and shape and were more densely packed than adjacent uncondensed mesenchyme (Figures 4, 5d, 6 and Table S4). Cells of condensation boundaries were bigger, more oblong in the direction of overlying epithelium (Figures 4b, 5d, 6b), and distinct from cells of adjacent mesenchyme, particularly in size and polarity

TABLE 2 | Protein expression and cell morphology in relation to tissue type, upper versus lower jaw, anterior–posterior, and dorsoventral zones and interactions among these factors prior ($t-1$) and during (t) condensation formation.

		Effects													
		Tissue		Jaw		ZoneAP		ZoneDV		Tissue*Jaw		Tissue*ZoneAP		Tissue*ZoneDV	
Factor	**Time**	***F***	***p***	***F***	***p***	***F***	***p***	***F***	***p***	***F***	***p***	***F***	***p***	***F***	***p***
β-catenin	t	**171.2**	< 0.01	0.1	0.71	**16.5**	< 0.01	0.2	0.81	**2.4**	0.05	**4.3**	< 0.01	1.8	0.07
	$t-1$	**6.8**	< 0.01	0.30	0.59	**4.7**	< 0.01	**9.4**	< 0.01	**3.1**	0.02	1.0	0.44	0.5	0.81
Bmp4	t	**11.7**	< 0.01	**4.6**	0.03	2.1	0.08	**6.5**	< 0.01	**2.5**	0.04	**4.2**	< 0.01	**5.7**	< 0.01
	$t-1$	**3.8**	< 0.01	**4.3**	0.04	0.6	0.65	**7.4**	< 0.01	**3.0**	0.02	0.9	0.53	1.9	0.06
CaM	t	**4.2**	< 0.01	**15.2**	< 0.01	**3.0**	0.02	0.9	0.39	0.3	0.90	1.5	0.11	**3.6**	< 0.01
	$t-1$	1.0	0.40	**17.8**	< 0.01	**7.1**	< 0.01	1.9	0.15	0.8	0.56	**2.6**	< 0.01	0.2	0.97
Dkk3	t	**2.9**	0.02	**6.4**	0.03	0.7	0.62	**4.1**	0.02	**5.5**	< 0.01	**2.6**	< 0.01	**3.0**	< 0.01
	$t-1$	**2.5**	0.04	3.1	0.15	2.1	0.09	**6.8**	< 0.01	**4.5**	< 0.01	1.1	0.36	1.2	0.31
Fgf8	t	**37.0**	< 0.01	**14.1**	< 0.01	**7.5**	< 0.01	**9.3**	< 0.01	**6.9**	< 0.01	**2.1**	0.01	**4.5**	< 0.01
	$t-1$	1.9	0.10	**6.3**	0.02	0.6	0.64	0.0	0.99	0.3	0.87	1.4	0.18	1.5	0.14
Ihh	t	**16.20**	< 0.01	**15.3**	< 0.01	**16.8**	< 0.01	**9.1**	< 0.01	**6.7**	< 0.01	**2.9**	< 0.01	**3.5**	< 0.01
	$t-1$	**2.9**	0.02	**17.1**	< 0.01	**6.1**	< 0.01	**9.7**	< 0.01	0.2	0.94	**3.2**	< 0.01	**2.2**	0.02
Tgfβ2	t	**26.7**	< 0.01	**8.0**	0.01	0.6	0.68	1.2	0.30	1.2	0.31	**1.9**	0.02	**2.3**	0.02
	$t-1$	1.7	0.15	1.0	0.34	0.9	0.44	**3.4**	0.04	1.4	0.23	1.3	0.21	**2.2**	0.03
Wnt4	t	**10.4**	< 0.01	**13.6**	< 0.01	**9.4**	< 0.01	**10.3**	< 0.01	**3.7**	< 0.01	**5.0**	< 0.01	**9.6**	< 0.01
	$t-1$	**6.0**	< 0.01	**12.0**	< 0.01	**2.4**	0.05	**5.8**	< 0.01	**2.4**	0.05	**2.3**	0.00	1.6	0.13
Roundness	t	**217.2**	< 0.01	**29.4**	< 0.01	**5.01**	< 0.01	**6.5**	< 0.01	**65.6**	< 0.01	**3.7**	< 0.01	**17.4**	< 0.01
	$t-1$	**15.5**	< 0.01	**282.7**	< 0.01	**5.5**	< 0.01	**10.4**	< 0.01	**13.6**	< 0.01	1.6	0.07	**2.0**	0.04
Size	t	**347.6**	< 0.01	**390.2**	< 0.01	**59.3**	< 0.01	**37.0**	< 0.01	**34.6**	< 0.01	**8.9**	< 0.01	**20.2**	< 0.01
	$t-1$	**31.7**	< 0.01	**75.7**	< 0.01	**2.4**	0.05	**53.8**	< 0.01	1.3	0.26	1.5	0.09	1.3	0.25
VarShape	t	**226.5**	< 0.01	**796.5**	< 0.01	**10.6**	< 0.01	**6.5**	< 0.01	**592.2**	< 0.01	**1.9**	0.02	**27.6**	< 0.01
	$t-1$	**12.3**	< 0.01	**259.4**	< 0.01	**4.5**	< 0.01	**9.8**	< 0.01	**20.7**	< 0.01	1.3	0.17	**4.5**	< 0.01
VarSize	t	**323.7**	< 0.01	**666.2**	< 0.01	**11.8**	< 0.01	**11.3**	< 0.01	**213.4**	< 0.01	**8.0**	< 0.01	**28.1**	< 0.01
	$t-1$	**27.5**	< 0.01	**117.9**	< 0.01	2.2	0.07	**31.9**	< 0.01	**9.3**	< 0.01	1.4	0.12	1.8	0.07
VarPolarity	t	**23.4**	< 0.01	**41.6**	< 0.01	**42.8**	< 0.01	**102.8**	< 0.01	**4.8**	< 0.01	**9.9**	< 0.01	**14.2**	< 0.01
	$t-1$	0.3	0.88	0.00	0.98	1.6	0.16	**18.1**	< 0.01	**5.1**	< 0.01	**1.5**	0.09	**2.0**	0.04
Density	t	**57.1**	< 0.01	**340.1**	< 0.01	**58.0**	< 0.01	**68.5**	< 0.01	**123.8**	< 0.01	**7.2**	< 0.01	**23.2**	< 0.01
	$t-1$	**11.3**	< 0.01	**162.2**	< 0.01	**23.1**	< 0.01	**10.1**	< 0.01	**5.5**	< 0.01	1.1	0.40	**4.8**	< 0.01

Note: Shown are Type III F values for fixed effects with variance components covariance structure and Kenward–Roger degrees of freedom from a mixed-effects model and associated p values. Bold values are significant at $p < 0.05$.

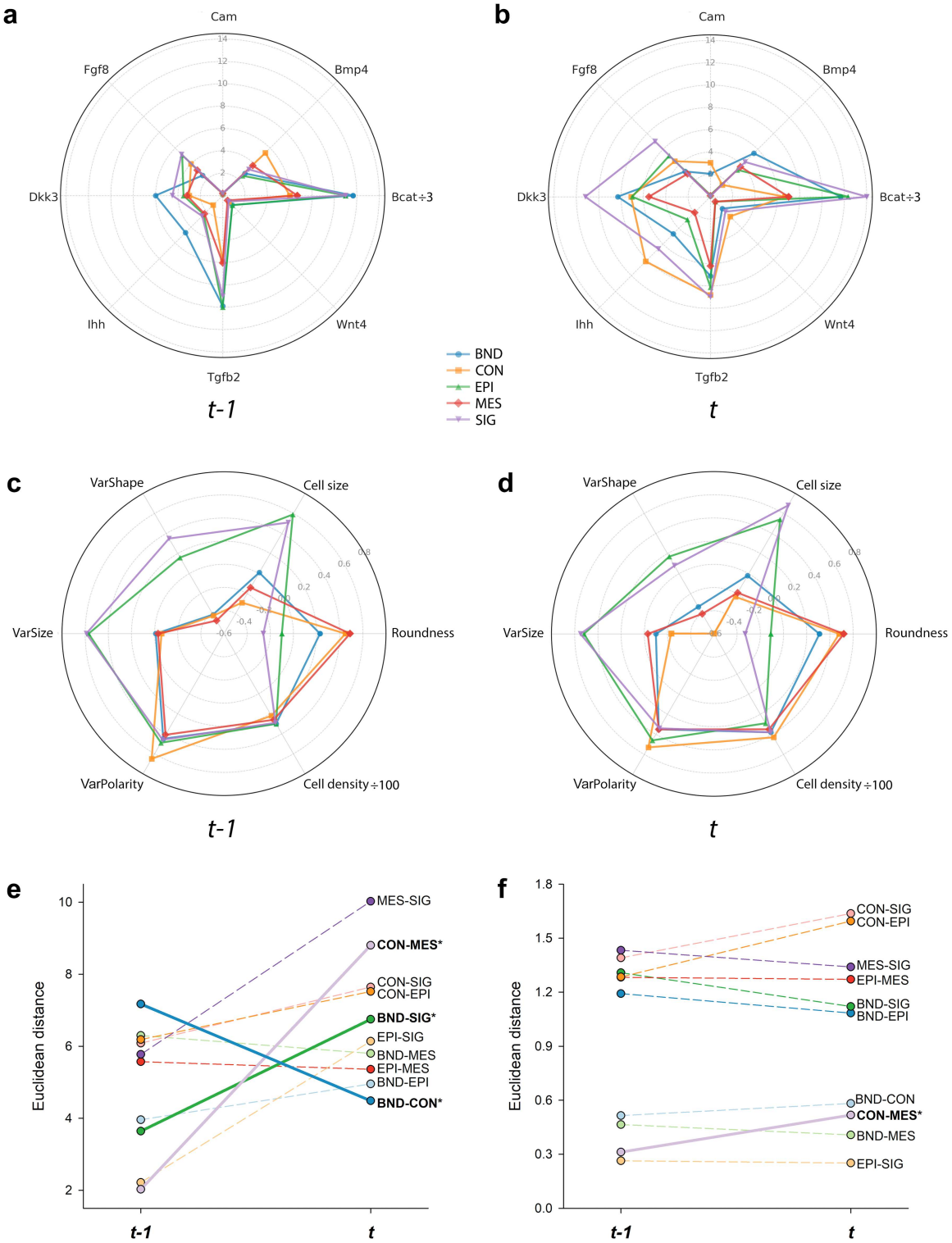

FIGURE 5 | Summary of tissue differences in (a and b) protein expression (β-catenin/3 is shown) and (c and d) cell morphology (cell density/100 is shown) as well as changes in pairwise tissue distances in (e) protein expression and (f) cell morphology between pre- ($t-1$) and condensation (t) stages (based on Figure 4). Bold values, solid lines, and asterisks indicate significant change in Euclidean distances (two-tailed t-test). [Color figure can be viewed at wileyonlinelibrary.com]

(Figure 5f) and in protein expression (Figures 4b, 5be and Table S4). The epithelium overlying condensations expressed higher Ihh and Wnt4 than the adjacent epithelium; uncondensed mesenchyme and its overlying epithelium differed in expression of all proteins, except for Dkk3 and Wnt4 (Figures 4, 5b and Tables 2, S4).

3.3 | Growing Condensations Undergo Cellular and Molecular Homogenization

Changes in molecular and cellular variation during condensation formation were mostly confined to condensed mesenchyme and its overlying epithelium (Figure 7 and Tables 3, S5). Bmp4 that was

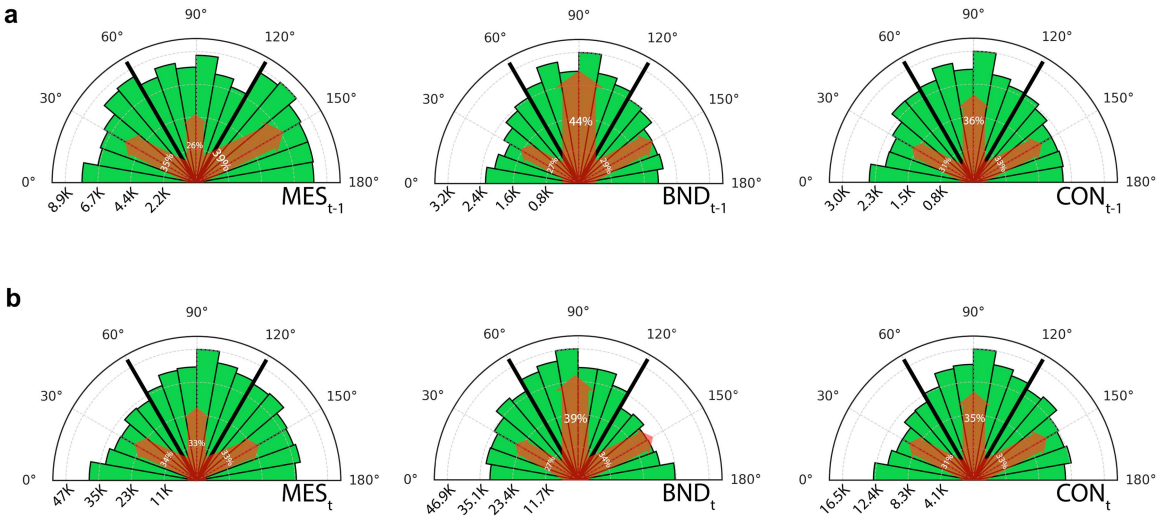

FIGURE 6 | Cell polarity in mesenchymal tissues (a) prior ($t-1$) and (b) during (t) condensation stage. 60°–120° tertile encompasses alignments toward or away from the adjacent epithelium. 0°–60° and 120°–180° tertiles encompass polarities toward or away from adjacent mesenchymal tissues (1/2 of the combined frequency should be used for direct comparison with the 60°–120° tertile frequency). The width of red arrows is proportional to the percentage of cells in the tertile. In precondensation stage ($t-1$), only boundary (BND) and mesenchyme (MES) differ from each other ($F_{2,18K} = 4.1$, $p = 0.02$, BND vs. MES, $p = 0.014$, Bonferroni-corrected $\alpha = 0.016$). During condensation stage (t), the polarity of all tissues differs from each other ($F_{2,18K} = 8.6$, $p < 0.001$, all pairwise p's < 0.01). [Color figure can be viewed at wileyonlinelibrary.com]

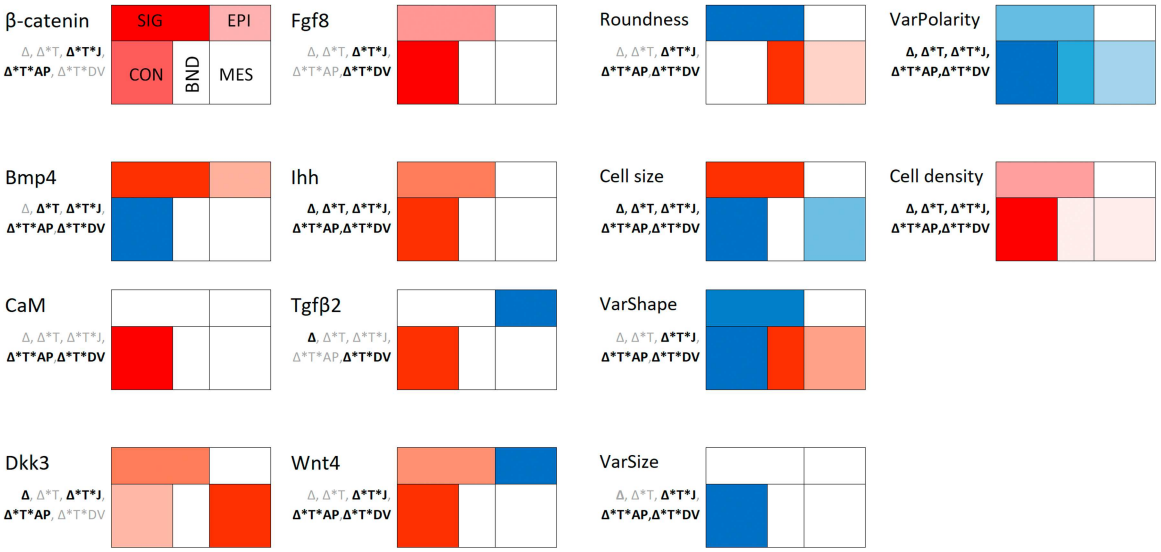

FIGURE 7 | Relative change [(after–before)/before] in protein expression and cell morphology between pre- ($t-1$) and condensation (t) stages (data in Table S5). Shown are LS means controlling for the effects of axial position, jaw, and population. Color saturation shows the magnitude of change (blue shows negative values, red shows positive values) among tissues within each protein or cell measure. Absence of color indicates a lack of significant change. Text shows significance of change (Δ) and its association with tissue type (Δ*T), jaw (Δ*T*J), anterior–posterior (Δ*T*AV), or dorsoventral (Δ*T*DV) axes. Bold values indicate significance at $\alpha < 0.05$ (Table 3). [Color figure can be viewed at wileyonlinelibrary.com]

highly expressed at the site of future condensations became non-detectable there, whereas expression of all other proteins increased strongly within condensations and the overlying epithelium (except for Tgfβ2 and CaM that only increased within the condensation) once a condensation was formed (Figure 7 and Tables 3, S5). β-catenin and Bmp4 also increased in the epithelium overlying uncondensed mesenchyme while Tgfβ2 and Wnt4 decreased; Dkk3 also became highly expressed in uncondensed mesenchyme (Figure 7 and Table S5). Within condensations, cells became smaller and more packed, more uniform in size and shape, and less polarized (Figures 4, 6, 7). Protein profiles of boundaries and condensations converged to each other while diverging from adjacent mesenchyme and epithelium (Figure 5a,b,e). Similarly, condensations became morphologically distinct from adjacent mesenchyme (Figure 5f).

3.4 | Axial Gradient and Local Specificity in Condensation Formation

Molecular and cellular changes during condensation formation were distinct between locations within the jaw and along AP

TABLE 3 | Context-dependence of change from precondensation to condensation stage in relation to tissue type, upper versus lower jaw, anterior–posterior, and dorsoventral zones.

	Effects									
	Time		Time*Tissue		Time*Tissue*Jaw		Time*Tissue*ZoneAP		Time*Tissue*ZoneDV	
Factor	***F***	***p***	***F***	***p***	***F***	***p***	***F***	***p***	***F***	***p***
β-catenin	0.0	0.96	0.9	0.47	**3.4**	< 0.01	**2.9**	< 0.01	1.9	0.05
Bmp4	1.6	0.21	**3.1**	0.01	**4.3**	< 0.01	**6.4**	< 0.01	**2.7**	< 0.01
CaM	0.7	0.40	1.3	0.26	1.3	0.25	**3.1**	< 0.01	**2.8**	< 0.01
Dkk3	**6.1**	0.01	0.7	0.59	**2.5**	0.01	**1.8**	0.02	1.6	0.11
Fgf8	0.2	0.70	0.4	0.83	**2.1**	0.03	1.3	0.21	**2.2**	0.02
Ihh	**11.1**	0.00	**4.2**	0.00	**15.7**	< 0.01	**6.9**	< 0.01	**9.2**	< 0.01
Tgfβ2	**14.1**	< 0.01	0.0	1.00	1.4	0.17	0.3	0.84	**2.2**	0.02
Wnt4	0.1	0.95	2.1	0.08	**2.9**	< 0.01	**2.9**	< 0.01	**4.4**	< 0.01
Roundness	0.5	0.50	1.1	0.37	**151.8**	< 0.01	**4.4**	< 0.01	**15.3**	< 0.01
Size	**23.0**	< 0.01	**2.6**	0.03	**19.6**	< 0.01	**6.6**	< 0.01	**10.4**	< 0.01
VarShape	2.4	0.12	1.3	0.26	**249.7**	< 0.01	**2.5**	< 0.01	**22.1**	< 0.01
VarSize	**4.4**	0.04	1.2	0.30	**97.6**	< 0.01	**3.0**	< 0.01	**19.7**	< 0.01
VarPolarity	**57.3**	< 0.01	**2.6**	0.03	**5.5**	< 0.01	**9.2**	< 0.01	**6.8**	< 0.01
Density	**33.3**	< 0.01	**14.7**	< 0.01	**82.4**	< 0.01	**4.0**	< 0.01	**19.9**	< 0.01

Note: Bold values are significant at $p < 0.05$. Statistics as in Table 2.

and DV axes (Figure 4 and Table 3). Prior to condensation formation, β-catenin, CaM, Ihh, Wnt4 and cell morphology, variability (except in polarity and size), and density formed a pronounced AP gradient in both jaws, while β-catenin, Bmp4, Dkk3, Ihh, Tgfβ2, Wnt4, and cell morphology, variability and density formed a DV gradient (Figure 4 and Table 2). Bmp4, CaM, Fgf8, Ihh, and Wnt4, along with cell morphology, density, and variability (except polarity), also differed strongly between upper and lower beak tissues prior to condensation formation (Table 2). Once a condensation was formed, cell morphology and variability depended on condensation location along the AP and DV axes, whereas many proteins showed positional variation along AV (except for Bmp4, Dkk3, and Tgfβ2) and DV (except for β-catenin, CaM, and Tgfβ2) axes and, particularly, between jaws (except for β-catenin, Table 2).

3.5 | Accumulation and Erasure of Local Specificity in Protein Expression During Condensation Formation

At the precondensation stage, proteins in the overlying epithelium and the mesenchyme of future condensation boundaries had the most locally specific expression; Dkk3, CaM, Ihh, Fgf8, and β-catenin had the most positional gradient dependency whereas Dkk3, β-catenin, and Wnt4 also had the most locally specific expression (Figures 8a, S4a and Table S6). Overall, cell morphology and variability were more associated with axial polarity and jaw placement and showed lesser local specificity than the protein expression (Figures 8b and S5). Among cell measures, shape covaried most closely with axial position in both jaws, whereas polarity and size were more locally specific (Figures 8, S5 and Table S6). As condensations grew, positional and locally specific variance in protein expression diminished within the condensation, its boundary, and the overlying epithelium, but not in the uncondensed mesenchyme or its adjacent epithelium (Figure 8a–d). Likewise, positional and locally specific variance in cell morphology declined as condensations grew, while increasing in uncondensed mesenchyme (Figure 8d). Once condensations formed, protein and cell variation in their mesenchyme had similar variance distribution across axes and jaw placements (Table S6).

4 | Discussion

We found that local specificity in avian beak mesenchymal condensations arises when some mesenchymal cells transiently match and propagate specific protein expression of the diverging overlying epithelium and become boundaries of future condensations (scenario f in Figure 1, Figure 9). Whereas signaling cross-talk between mesenchymal cells and overlying epithelium is known to drive condensation placement (Brito et al. 2008; Francis-West et al. 1994; B. K. Hall and Miyake 1992; Haworth et al. 2004; Kumar et al. 2012; LaMantia et al. 2000; S.-H. Lee et al. 2021; Mina et al. 2002; Richman and Tickle 1989; Xu et al. 2023), here we present the temporally resolved dynamics of this process and show how it determines specificity of condensation placement. Our results directly implicate the mesenchymal boundary of condensations as a key anchoring mechanism that allows mesenchyme to maintain and internalize initial epithelium signaling, sustaining reciprocal cross-talk between the two tissues (e.g., He et al. 2025). We also find that the local matching phase is brief as accumulating NCM cells progressively erase shared locally specific variation and restore their region- and tissue-specific protein profiles.

These findings raise three key questions. First, what are the mechanisms by which NCM and epithelial cells share their

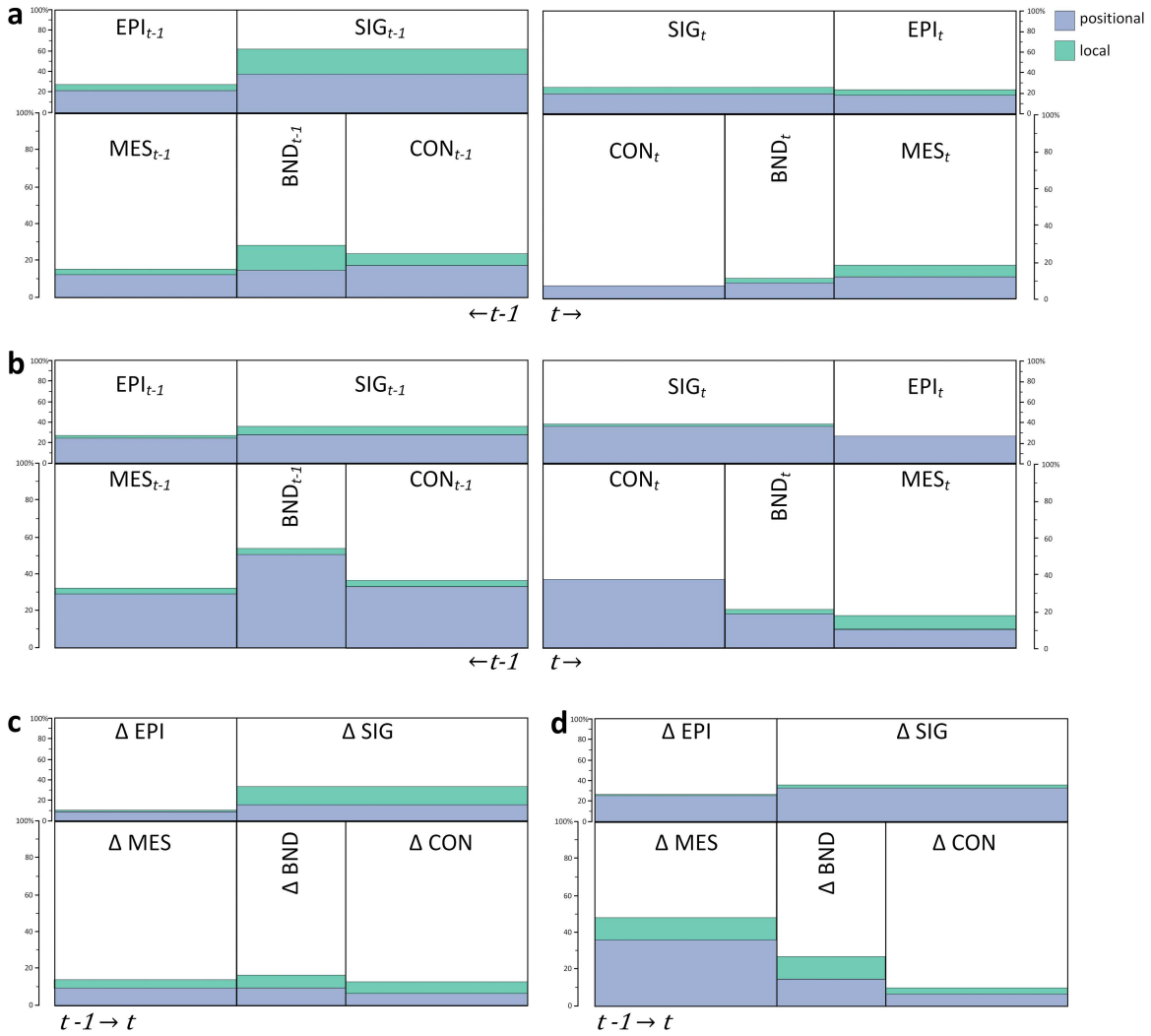

FIGURE 8 | Distribution of positional (blue) and local (green) variance (%) between pre ($t-1$) and condensation (t) stages in (a) protein expression and (b) cell morphology and variability measures (averages for cellular and molecular contributions) and changes associated with condensation formation in focal tissues in (c) protein expression, and (d) cellular measures. Data in Table S6; Figures S4 and S5. [Color figure can be viewed at wileyonlinelibrary.com]

protein profiles, and how is location specificity of these profiles originated? Second, how do accumulating NCM cells erase this location specificity with cell accumulation (Figure 8c,d). Of particular relevance is the relationship between the number of accumulating cells and their ability to maintain their uniformity. Third, what enables the conserved regulatory proteins studied here to drive highly context-specific and often sequentially opposite histological changes during condensation origin and differentiation? (Figure 4).

Several molecular and epigenetic mechanisms could account for the transient signal mimicry of overlying epithelium by the adjacent mesenchyme. First, the multipotent NCM cells at the sites of future condensations express an array of transcription factors able to respond to epithelial cues and also possess the open chromatin architecture making epithelial-like enhancers accessible (e.g., Selleri and Rijli 2023; Van Otterloo et al. 2022). This poised state can enable NCM cells to match local combinations of signaling ligands under epithelial induction. Under this scenario, NCM cells receiving an epithelial signal activate a transcriptional program similar to the epithelial source (Francis-West et al. 1994; Hu et al. 2015; Kumar et al. 2012; Xavier et al. 2016; Xu et al. 2023). This acquired autonomous signaling, in turn, either amplifies signaling through feedback to the epithelium or propagates the signal further into the mesenchyme (Figure 9) (Brito et al. 2008; Hu et al. 2015; Xavier et al. 2016).

Second, the transient epithelium–mesenchyme matching might involve morphogen transport between cells, by either specialized structures or through active cell rearrangement or outgrowth (e.g., Kicheva and Briscoe 2023). For example, cytonemes can directly deliver proteins through cell membrane contacts and transport receptors (Daly et al. 2022; Kornberg and Roy 2014; Wood et al. 2021). Observations that boundary cells are strongly polarized toward the overlying epithelium (Figure 6a) and form denser aggregations (Figure 4b) are consistent with cytoneme-based or filopodial-contact protein transfer rather than passive diffusion. Cytomeres can carry multiple proteins across cell contacts at once, explaining how Ihh, β-catenin, Bmp4, and Dkk3 are simultaneously matched in mesenchyme (Figure 4a). Similarly, extracellular exosomes can

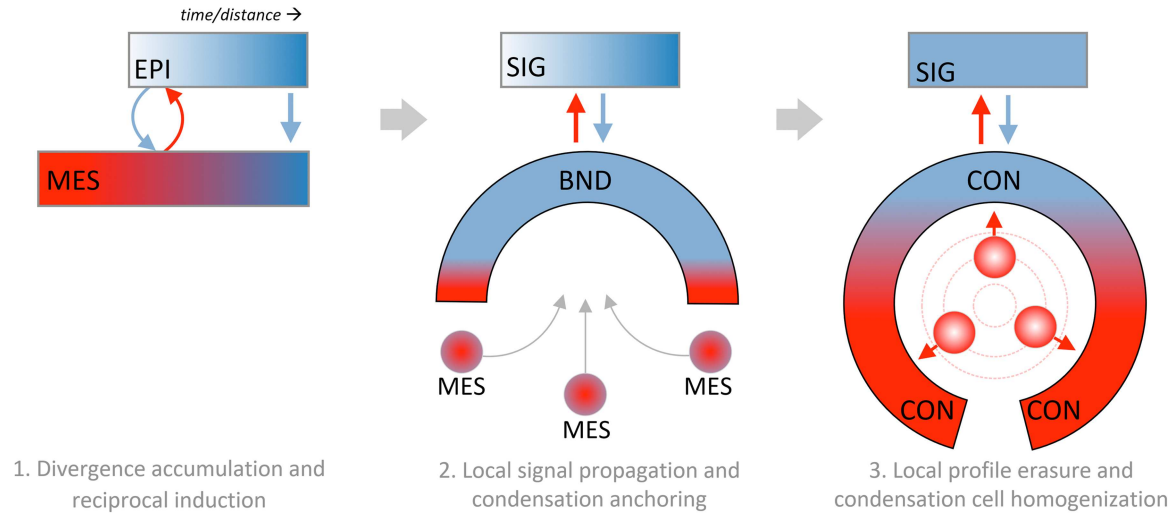

FIGURE 9 | Hypothetical scenario reconciling location specificity and multipotentiality retention in cell condensation most consistent with the results of this study (Figure 1f). Reciprocal signaling induction between postmigratory NCM cells and diverging overlying epithelium (Figures 4 and 5) leads to signal propagation and internalization by mesenchyme (Figure 6), enabling specific anchoring of condensation. Accumulating cells in forming condensations undergo homogenization and erase locally specific factor expression (Figure 8). Tissue abbreviations as in Figure 1. [Color figure can be viewed at wileyonlinelibrary.com]

diffuse through the basement membrane between epithelial and mesenchymal cells (Conigliaro and Cicchini 2019; Jiang et al. 2017). These vesicles can transfer not only proteins, but also mRNAs and miRNAs, effectively reprogramming boundary cells. This mechanism could account for the rapid and transient adoption of epithelial-like expression in condensation boundary cells without requiring transcriptional activation.

Strong polarization of future boundary cells toward the overlying epithelium (Figure 6a) and these cells' propensity to form denser aggregations (Figure 4b), raises the possibility that the observed epithelial signaling propagation is produced by mesenchymal cellular outgrowth. Interestingly, the mesenchyme of future boundaries had a similar protein profile to the overlying epithelium, but distinct protein expression and polarization to its adjacent mesenchyme, including that of the future condensation (Figure 5e), implying that it is the mesenchyme that extends the epithelial signaling and not the other way around. This directionality is corroborated by the finding that protein profiles of signaling epithelium increasingly diverge from other tissues, whereas those of condensation boundaries converge with other tissues as condensation forms (Figure 5e). Cell jamming transitions that occur ubiquitously in precondensation mesenchyme of these samples and are directly linked to protein propagation (Badyaev et al. 2025) could account for distinct material properties of dense boundary cells that facilitate signal internalization and local compartmentalization.

The finding that the signaling mimicry between adjacent tissues differs between locations (Figure 8) suggests that the location specificity of NCM cell condensations is a by-product of their cross-talk with local epithelium. Under this scenario, the initial anchoring of a mesenchymal condensation by epithelial mimicry is reinforced by mesenchyme's own propagation and amplification of local signaling (Figure 9). A combination of molecular memory in groups of NCM cells accumulated during migration, and developmental divergence of local epithelium (Figure 1a) produces a unique signaling combination; signal matching between the two adjacent tissues could thus produce locally specific condensation anchoring by default (Eames and Schneider 2008; Kaucka et al. 2016; Palmquist et al. 2022; Selleri and Rijli 2023; Welsh and O'Brien 2009; Wu et al. 2006). This mechanism can scale up to the level of axial placement of condensations as long as the epithelial–mesenchymal feedback involves the induction of the signaling boundary of a future condensation. For example, in the frontonasal ectodermal zone in avian embryos a mesenchymal signaling boundary is formed at the interface of Fgf8 and Shh domains of the overlying epithelium (Foppiano et al. 2007; Hu et al. 2003; Lu et al. 2024). Similar scenarios (Figure 8) occur in bidirectional epithelial–mesenchymal feedback of WNT/β-catenin signaling (Reid et al. 2011). In both of these examples, local matching of the adjacent tissues is enabled by modulations of a conserved regulatory network by time- and distance-dependent cell proliferation and migration. Notably, the observed location specificity of protein profiles is brief and rapidly replaced by general positional and tissue-specific protein expressions as condensations grow (Figure 8c,d and Table S6). This echoes a classical finding that the initial matching phase of epithelial signaling is short and stage-specific, whereas the subsequent amplification and divergence of signaling by condensed mesenchyme must be prolonged to maintain condensations despite divergence of surrounding tissues (B. K. Hall and Miyake 1992). Essentially, the boundary allows condensed mesenchyme to internalize the epithelial signaling.

Distance to the boundaries also determines the rate of cellular and molecular homogenization within condensations and the onset of cell differentiation once this uniformity cannot be maintained after a condensation reaches a certain size (Cottrill et al. 1987; B. K. Hall and Miyake 1992). We observed that the acquisition of molecular uniformity coincides with cellular transformation – condensation cells became smaller and more uniform in size, shape, and polarity as they acquire similar

protein expression (Figures 5, 7, 8 and Tables 3, S6). Within condensations, cell uniformity is maintained through self-referencing and competition; the ability to mix and move is key to this process (Kaucka et al. 2016; Shahbazi et al. 2017; Zheng et al. 2021). Once cell movement is restricted, the condensation's size could determine the onset and range of differentiation (Badyaev et al. 2025).

The proteins studied here are involved in a multitude of cellular and histological processes of avian beak development (Betancur et al. 2010; Cheng et al. 2024; Wu et al. 2004), composing a core regulatory network able to produce an array of configurations with context-dependent effects on cellular dynamics (Badyaev et al. 2026; Duckworth et al. 2025; Mallarino et al. 2012). Our results strongly corroborate the role of Ihh as a boundary-specifying signal that predates the morphological appearance of cell condensation; it is essential in delineating condensations and synchronizing accumulating condensation cells (Amano et al. 2020; Colnot et al. 2005). In agreement with other studies, we also found key involvement of Bmp4, Fgf8, and CaM in the origin of condensations (B. K. Hall and Miyake 2000; Minoux and Rijli 2010; Santagati and Rijli 2003; Svandova et al. 2020). For example, Bmp4 was upregulated at sites of future condensations (Figure 4b and Table S4), where it promotes cell proliferation and cell compaction, whereas the strong upregulation of Fgf8 can prevent cell apoptosis at adjacent tissues in addition to providing positional information (Barna and Niswander 2007; B. K. Hall and Miyake 2000; Hu and Marcucio 2009; Minoux and Rijli 2010; Santagati and Rijli 2003; Wu et al. 2004, 2006). Interestingly, Bmp4 was sharply downregulated once condensations started to form (but upregulated in their boundaries, Figure 4a), likely to delay cell differentiation before the condensation reaches full size, as the presence of Bmp4 is associated with chondrogenesis and osteogenesis especially when coupled with high Ihh expression as found here (Figure 3a) (Celá et al. 2016; Giffin et al. 2019; Kobayashi et al. 2005; Mallarino et al. 2012; Wu et al. 2006; Yoon et al. 2006).

Context- and time-specific modulation of the protein network can explain some discrepancies between our and previous studies. For example, a downregulation of mesenchymal Tgfβ2 was found to be required for condensation formation (Ray and Chapman 2015), whereas we found a strong upregulation of this protein immediately prior to condensation formation in the tissues of the future boundary and overlying epithelium followed by an upregulation in condensing mesenchyme (Figures 4a, 5a and Table S4). Although, similarly to Bmp4, downregulation of Tgfβ2 can delay the onset of cell differentiation within condensations and prevent the formation of linkages to Bmp4 and Wnt4 that promote osteogenesis (Ray and Chapman 2015), here Tgfβ2's increase can be explained by its upregulation of CaM, which is essential for cell adhesion and compaction in the formation of condensation boundaries (Figures 4a, 5a and Table S4) (B. K. Hall and Miyake 2000; Lin et al. 2006; Widelitz et al. 1993). The mechanochemical framework supports this interpretation: actomyosin-driven condensation simultaneously activates Bmp4/Fgf8 while suppressing Tgfβ2 in established condensations, suggesting a temporal switch (He et al. 2025). Interestingly, Bmp4 and Tgfβ2 expression had the lowest positional and locally specific variance, indicating their persistent global effects compared to other proteins under this study (Figure S4). Similarly, a strong upregulation of β-catenin within future condensation boundaries was consistently associated with cell polarized aggregation and compaction (Figure 4), whereas β-catenin increase in the overlying epithelium (Figure 4a) suggests mechanical reorganization of epithelial tissues (e.g., Palmquist et al. 2022; Shyer et al. 2017).

Our results also shed light on the long-range cellular processes contributing to condensation formation (scenarios *ii* and *iii* in Figure 3b are supported by our findings). Accumulating cell density within condensations was accompanied by a decrease of cell density in the surrounding mesenchyme (Figures 2 and 3) which, in combination with the strong lateral polarity of mesenchymal tissues adjacent to condensations (Figure 6a), suggests that cell migration contributes to condensation formation and cell compaction (Figure 3a). Further, condensation formation is associated with a relative increase in cell proliferation at the condensation site and the associated decrease in average cell size and variability (Figure 7), corroborating previous findings (Abramyan and Richman 2015; Barna and Niswander 2007; Brembeck et al. 2006; Giffin et al. 2019; B. K. Hall and Miyake 2000; J. Hall et al. 2014; Paudel et al. 2022; Wu et al. 2006).

Cell polarity affects the orientation of cell division and cell migration and plays a key role in tissue reorganization during craniofacial development (e.g., Li et al. 2017; Yamaguchi et al. 1999). β-catenin-independent Wnt pathways affect cell polarity (Gao et al. 2011; Ho et al. 2012; Konopelski Snavely et al. 2023) and we found that distinct Wnt4 expression in the boundary, condensation, and uncondensed mesenchyme corresponded to divergent cell polarity in these tissues (Figures 4, 5b, 6). Furthermore, the formation of condensations was associated with the reversal in Wnt4 expression between signaling and adjacent epithelium (Figure 7), corresponding to a signaling boundary between adjacent mesenchymal tissues with orthogonal polarity (Figure 6).

In sum, the developmental organization revealed here could reconcile the multipotentiality of NCM cells, evolutionarily conserved epithelial-mesenchymal signaling, and the regional specificity of cell condensations placement needed for proper development. Because the juxtaposition and growth dynamics of cell condensations ultimately determine evolutionary diversification in avian beak shapes and sizes (Abzhanov et al. 2004, 2006; Badyaev 2011; Campàs et al. 2010; Linde-Medina et al. 2016; Schneider 2024; Wu et al. 2004), the mechanisms underlying the onset and erasure of position specificity in NCM stem cells are likely to be central in this process.

Acknowledgments

This study was inspired by the lifelong scientific contributions of Dr. Brian K. Hall, who also provided insightful suggestions on the approaches used in this study and helped frame key concepts. It is an honor to dedicate this paper to him. The authors are also grateful to R. A. Duckworth, T. Franz-Odendaal, H. Gee, M. Jenkins, S. Cooke, G. Fraser, and anonymous reviewers for their extensive comments and suggestions on previous versions of this manuscript. This work was

supported by the grants from the National Science Foundation (IBN-0218313 and DEB-1754465) to A.V.B., as well as NSF REU, Tindall Memorial Research Fellowship, Silliman Memorial Research Fellowships, Galileo Circle Scholarships, and the Science Deans Innovation Award to C.S.M.

Ethics Statement

All sampling for this work was conducted under US Federal Permit (23182), US Federal Collecting Permit (MB24327C-0), annual state permits for Montana (2016-098, 15-0-20-W) and Arizona (SP637758), and approved by the Institutional Animal Care and Use Committee of the University of Arizona (13-423).

Conflicts of Interest

The authors declare no conflicts of interest.

Data Availability Statement

All data and the analyses are in the manuscript and the Supporting Materials.

References

Abramyan, J., and J. M. Richman. 2015. "Recent Insights Into the Morphological Diversity in the Amniote Primary and Secondary Palates." *Developmental Dynamics* 244, no. 12: 1457–1468. https://doi.org/10.1002/dvdy.24338.

Abzhanov, A., W. P. Kuo, C. Hartmann, B. R. Grant, P. R. Grant, and C. J. Tabin. 2006. "The Calmodulin Pathway and Evolution of Elongated Beak Morphology in Darwin's Finches." *Nature* 442: 563–567.

Abzhanov, A., M. Protas, B. R. Grant, P. R. Grant, and C. J. Tabin. 2004. "*Bmp4* and Morphological Variation of Beaks in Darwin's Finches." *Science* 305: 1462–1464.

Akieda, Y., S. Ogamino, H. Furuie, et al. 2019. "Cell Competition Corrects Noisy Wnt Morphogen Gradients to Achieve Robust Patterning in the Zebrafish Embryo." *Nature Communications* 10, no. 1: 4710. https://doi.org/10.1038/s41467-019-12609-4.

Amano, K., D. Okuzaki, T. Aikawa, and M. Kogo. 2020. "Indian Hedgehog in Craniofacial Neural Crest Cells Links to Skeletal Malocclusion by Regulating Associated Cartilage Formation and Gene Expression." *FASEB Journal* 34, no. 5: 6791–6807. https://doi.org/10.1096/fj.201903269R.

Atchley, W. R., and B. K. Hall. 1991. "A Model for Development and Evolution of Complex Morphological Structures." *Biological Reviews* 66: 101–157.

Badyaev, A. V. 2010. "The Beak of the Other Finch: Coevolution of Genetic Covariance Structure and Developmental Modularity During Adaptive Evolution." *Philosophical Transactions of the Royal Society, B: Biological Sciences* 365: 1111–1126.

Badyaev, A. V. 2011. "How Do Precise Adaptive Features Arise in Development? Examples With Evolution of Context-Specific Sex-Ratios and Perfect Beaks." *Auk* 128: 467–474.

Badyaev, A. V., C. A. Lee, M. J. Gleason, et al. 2025. "Cell Jamming Transitions Can Affect Regulatory Protein Gradients and Prime Evolutionary Divergence." *Journal of the Royal Society Interface* 22: 20250186. https://doi.org/10.1098/rsif.2025.0186.

Badyaev, A. V., C. Sánchez Moreno, C. A. Lee, S. E. Britton, L. M. Johnstone, and R. A. Duckworth. 2026. "Ultimate Paths of Least Resistance: Intrinsically Disordered Proteins as Developmental Resets in Regulatory Networks." *Proceedings of the Royal Society B: Biological Sciences* 293, no. 2062: 20252393. https://doi.org/10.1098/rspb.2025.2393.

Barna, M., and L. Niswander. 2007. "Visualization of Cartilage Formation: Insight Into Cellular Properties of Skeletal Progenitors and Chondrodysplasia Syndromes." *Developmental Cell* 12, no. 6: 931–941. https://doi.org/10.1016/j.devcel.2007.04.016.

Barriga, E. H., K. Franze, G. Charras, and R. Mayor. 2018. "Tissue Stiffening Coordinates Morphogenesis by Triggering Collective Cell Migration In Vivo." *Nature* 554, no. 7693: 523–527. https://doi.org/10.1038/nature25742.

Betancur, P., M. Bronner-Fraser, and T. Sauka-Spengler. 2010. "Assembling Neural Crest Regulatory Circuits Into a Gene Regulatory Network." *Annual Review of Cell and Developmental Biology* 26: 581–603. https://doi.org/10.1146/annurev.cellbio.042308.113245.

Brembeck, F. H., M. Rosário, and W. Birchmeier. 2006. "Balancing Cell Adhesion and Wnt Signaling, the Key Role of Beta-Catenin." *Current Opinion in Genetics & Development* 16, no. 1: 51–59. https://doi.org/10.1016/j.gde.2005.12.007.

Brito, M., M. Teillet, and N. M. Le Douarin. 2008. "Induction of Mirror-Image Supernumerary Jaws in Chicken Mandibular Mesenchyme by Sonic Hedgehog-Producing Cells." *Development* 135, no. 13: 2311–2319. https://doi.org/10.1242/dev.019125.

Buitrago-Delgado, E., K. Nordin, A. Rao, L. Geary, and C. LaBonne. 2015. "Shared Regulatory Programs Suggest Retention of Blastula-Stage Potential in Neural Crest Cells." *Science* 348: 1332–1335.

Campàs, O., R. Mallarino, A. Herrel, A. Abzhanov, and M. P. Brenner. 2010. "Scaling and Shear Transformations Capture Beak Shape Variation in Darwin's Finches." *Proceedings of the National Academy of Sciences of the United States of America* 107: 3356–3360.

Celá, P., M. Buchtová, I. Veselá, et al. 2016. "BMP Signaling Regulates the Fate of Chondro-Osteoprogenitor Cells in Facial Mesenchyme in a Stage-Specific Manner." *Developmental Dynamics* 245, no. 9: 947–962. https://doi.org/10.1002/dvdy.24422.

Cheng, Y., M. J. Miller, and F. Lei. 2024. "Molecular Innovations Shaping Beak Morphology in Birds." *Annual Review of Animal Biosciences* 13: 99–119. https://doi.org/10.1146/annurev-animal-030424-074906.

Colnot, C., L. de la Fuente, S. Huang, et al. 2005. "Indian Hedgehog Synchronizes Skeletal Angiogenesis and Perichondrial Maturation With Cartilage Development." *Development* 132, no. 5: 1057–1067. https://doi.org/10.1242/dev.01649.

Conigliaro, A., and C. Cicchini. 2019. "Exosome-Mediated Signaling in Epithelial to Mesenchymal Transition and Tumor Progression." *Journal of Clinical Medicine* 8, no. 1: 26. https://doi.org/10.3390/jcm8010026.

Cottrill, C. P., C. W. Archer, and L. Wolpert. 1987. "Cell Sorting and Chondrogenic Aggregate Formation in Micromass Culture." *Developmental Biology* 122: 503–515. https://doi.org/10.1016/0012-1606(87)90314-9.

Creuzet, S., G. Couly, and N. M. Le Douarin. 2005. "Patterning the Neural Crest Derivatives During Development of the Vertebrate Head: Insights From Avian Studies." *Journal of Anatomy* 207, no. 5: 447–459. https://doi.org/10.1111/j.1469-7580.2005.00485.x.

Daly, C. A., E. T. Hall, and S. K. Ogden. 2022. "Regulatory Mechanisms of Cytoneme-Based Morphogen Transport." *Cellular and Molecular Life Sciences* 79, no. 2: 119. https://doi.org/10.1007/s00018-022-04148-x.

Depew, M. J., and C. Compagnucci. 2008. "Tweaking the Hinge and Caps: Testing a Model of the Organization of Jaws." *Journal of Experimental Zoology Part B: Molecular and Developmental Evolution* 310, no. 4: 315–335. https://doi.org/10.1002/jez.b.21205.

Duckworth, R. A., S. E. Britton, C. A. Lee, K. C. Chenard, and A. V. Badyaev. 2025. "Spatial and Temporal Coordination of Signaling Pathways in Tissue Differentiation: Developmental Atlas of Protein Expression During Zebra Finch Beak Maturation." Preprint, *BioRxiv*: 2025.2012.2017.695020. https://doi.org/10.64898/2025.12.17.695020.

Dunlop, L. L., and B. K. Hall. 1995. "Relationships Between Cellular Condensation, Preosteoblast Formation and Epithelial-Mesenchymal

Interactions in Initiation of Osteogenesis." *International Journal of Developmental Biology* 39, no. 2: 357–371.

Dupin, E., G. W. Calloni, J. M. Coelho-Aguiar, and N. M. Le Douarin. 2018. "The Issue of the Multipotency of the Neural Crest Cells." *Developmental Biology* 444, no. Suppl 1: S47–S59. https://doi.org/10.1016/j.ydbio.2018.03.024.

Eames, B. F., and J. A. Helms. 2004. "Conserved Molecular Program Regulating Cranial and Appendicular Skeletogenesis." *Developmental Dynamics* 231, no. 1: 4–13. https://doi.org/10.1002/dvdy.20134.

Eames, B. F., and R. A. Schneider. 2008. "The Genesis of Cartilage Size and Shape During Development and Evolution." *Development* 135: 3947–3958.

Fonseca, B. F., G. Couly, and E. Dupin. 2017. "Respective Contribution of the Cephalic Neural Crest and Mesoderm to SIX1-Expressing Head Territories in the Avian Embryo." *BMC Developmental Biology* 17, no. 1: 13. https://doi.org/10.1186/s12861-017-0155-z.

Foppiano, S., D. Hu, and R. S. Marcucio. 2007. "Signaling by Bone Morphogenetic Proteins Directs Formation of an Ectodermal Signaling Center That Regulates Craniofacial Development." *Developmental Biology* 312, no. 1: 103–114. https://doi.org/10.1016/j.ydbio.2007.09.016.

Francis-West, P., R. Ladher, A. Barlow, and A. Graveson. 1998. "Signalling Interactions During Facial Development." *Mechanisms of Development* 75: 3–28.

Francis-West, P. H., T. Tatla, and P. M. Brickell. 1994. "Expression Patterns of the Bone Morphogenetic Protein Genes Bmp-4 and Bmp-2 in the Developing Chick Face Suggest a Role in Outgrowth of the Primordia." *Developmental Dynamics* 201, no. 2: 168–178. https://doi.org/10.1002/aja.1002010207.

Fritz, J. A., J. Brancale, M. Tokita, et al. 2014. "Shared Developmental Programme Strongly Constrains Beak Shape Diversity in Songbirds." *Nature Communications* 5: 3700. https://doi.org/10.1038/ncomms4700.

Gao, B., H. Song, K. Bishop, et al. 2011. "Wnt Signaling Gradients Establish Planar Cell Polarity by Inducing Vangl2 Phosphorylation Through Ror2." *Developmental Cell* 20: 163–176.

Giffin, J. L., D. Gaitor, and T. A. Franz-Odendaal. 2019. "The Forgotten Skeletogenic Condensations: A Comparison of Early Skeletal Development Amongst Vertebrates." *Journal of Developmental Biology* 7, no. 1: 4. https://doi.org/10.3390/jdb7010004.

Gitton, Y., E. Heude, M. Vieux-Rochas, et al. 2010. "Evolving Maps in Craniofacial Development." *Seminars in Cell & Developmental Biology* 21, no. 3: 301–308. https://doi.org/10.1016/j.semcdb.2010.01.008.

Glimm, T., R. Bhat, and S. A. Newman. 2014. "Modeling the Morphodynamic Galectin Patterning Network of the Developing Avian Limb Skeleton." *Journal of Theoretical Biology* 346: 86–108. https://doi.org/10.1016/j.jtbi.2013.12.004.

Hall, B. K. 1978. *Developmental and Cellular Skeletal Biology*. Academic Press.

Hall, B. K. 1980. "Tissue Interactions and the Initiation of Osteogenesis and Chondrogenesis in the Neural Crest-Derived Mandibular Skeleton of the Embryonic Mouse as Seen in Isolated Murine Tissues and in Recombinations of Murine and Avian Tissues." *Development* 58: 251–264.

Hall, B. K. 1999. *The Neural Crest in Development and Evolution*. Springer-Verlag.

Hall, B. K. 2003. "Unlocking the Black Box Between Genotype and Phenotype: Cell Condensations as Morphogenetic (Modular) Units." *Biology and Philosophy* 18: 219–247.

Hall, B. K. 2018. "Germ Layers, the Neural Crest and Emergent Organization in Development and Evolution." *Genesis* 56, no. 6–7: e23103. https://doi.org/10.1002/dvg.23103.

Hall, J., A. H. Jheon, E. L. Ealba, et al. 2014. "Evolution of a Developmental Mechanism: Species-Specific Regulation of the Cell Cycle and the Timing of Events During Craniofacial Osteogenesis." *Developmental Biology* 385, no. 2: 380–395. https://doi.org/10.1016/j.ydbio.2013.11.011.

Hall, B. K., and T. Miyake. 1992. "The Membranous Skeleton: The Role of Cell Condensations in Vertebrate Skeletogenesis." *Anatomy and Embryology* 186: 107–124.

Hall, B. K., and T. Miyake. 2000. "All for One and One for All: Condensations and the Initiation of Skeletal Development." *BioEssays* 22: 138–147.

Haworth, K. E., C. Healy, P. Morgan, and P. T. Sharpe. 2004. "Regionalisation of Early Head Ectoderm Is Regulated by Endoderm and Prepatterns the Orofacial Epithelium." *Development* 131: 4797–4806.

He, J. X., B. D. Sui, Y. Jin, C. X. Zheng, and F. Jin. 2025. "Cell Condensation Initiates Organogenesis: The Role of Actin Dynamics in Supracellular Self-Organizing Process." *Cell & Bioscience* 15, no. 1: 101. https://doi.org/10.1186/s13578-025-01429-3.

Ho, H.-Y. H., M. W. Susman, J. B. Bikoff, et al. 2012. "Wnt5a-Ror-Dishevelled Signaling Constitutes a Core Developmental Pathway That Controls Tissue Morphogenesis." *Proceedings of the National Academy of Sciences* 109: 4044–4051.

Hovland, A. S., D. Bhattacharya, A. P. Azambuja, et al. 2022. "Pluripotency Factors Are Repurposed to Shape the Epigenomic Landscape of Neural Crest Cells." *Developmental Cell* 57, no. 19: 2257–2272.e5. https://doi.org/10.1016/j.devcel.2022.09.006.

Hu, D., and R. S. Marcucio. 2009. "Unique Organization of the Frontonasal Ectodermal Zone in Birds and Mammals." *Developmental Biology* 325: 200–210.

Hu, D., and R. S. Marcucio. 2012. "Neural Crest Cells Pattern the Surface Cephalic Ectoderm During FEZ Formation." *Developmental Dynamics* 241, no. 4: 732–740. https://doi.org/10.1002/dvdy.23764.

Hu, D., R. S. Marcucio, and J. A. Helms. 2003. "A Zone of Frontonasal Ectoderm Regulates Patterning and Growth in the Face." *Development* 130, no. 9: 1749–1758. https://doi.org/10.1242/dev.00397.

Hu, D., N. M. Young, X. Li, Y. Xu, B. Hallgrímsson, and R. S. Marcucio. 2015. "A Dynamic Shh Expression Pattern, Regulated by SHH and BMP Signaling, Coordinates Fusion of Primordia in the Amniote Face." *Development* 142, no. 3: 567–574. https://doi.org/10.1242/dev.114835.

Hu, D., N. M. Young, Q. Xu, et al. 2015. "Signals From the Brain Induce Variation in Avian Facial Shape." *Developmental Dynamics* 244, no. 9: 1133–1143. https://doi.org/10.1002/dvdy.24284.

Jheon, A. H., and R. A. Schneider. 2009. "The Cells That Fill the Bill: Neural Crest and the Evolution of Craniofacial Development." *Journal of Dental Research* 88: 12–21.

Jiang, N., L. Xiang, L. He, et al. 2017. "Exosomes Mediate Epithelium-Mesenchyme Crosstalk in Organ Development." *ACS Nano* 11, no. 8: 7736–7746. https://doi.org/10.1021/acsnano.7b01087.

Kaucka, M., E. Ivashkin, D. Gyllborg, et al. 2016. "Analysis of Neural Crest–Derived Clones Reveals Novel Aspects of Facial Development." *Science Advances* 2: e1600060.

Kaul, H., B. K. Hall, C. Newby, and Y. Ventikos. 2015. "Synergistic Activity of Polarised Osteoblasts Inside Condensations Cause Their Differentiation." *Scientific Reports* 5: 11838. https://doi.org/10.1038/srep11838.

Kelsh, R. N., K. Camargo Sosa, S. Farjami, V. Makeev, J. H. P. Dawes, and A. Rocco. 2021. "Cyclical Fate Restriction: A New View of Neural Crest Cell Fate Specification." *Development* 148, no. 22: dev176057. https://doi.org/10.1242/dev.176057.

Kicheva, A., and J. Briscoe. 2023. "Control of Tissue Development by Morphogens." *Annual Review of Cell and Developmental Biology* 39: 91–121. https://doi.org/10.1146/annurev-cellbio-020823-011522.

Kobayashi, T., K. M. Lyons, A. P. McMahon, and H. M. Kronenberg. 2005. "BMP Signaling Stimulates Cellular Differentiation at Multiple Steps During Cartilage Development." *Proceedings of the National Academy of Sciences* 102, no. 50: 18023–18027.

Konopelski Snavely, S. E., S. Srinivasan, C. A. Dreyer, J. Tan, K. L. Carraway, and H.-Y. H. Ho. 2023. "Non-Canonical WNT5A-ROR Signaling: New Perspectives on an Ancient Developmental Pathway." *Current Topics in Developmental Biology* 153: 195–227.

Kornberg, T. B., and S. Roy. 2014. "Cytonemes as Specialized Signaling Filopodia." *Development* 141, no. 4: 729–736. https://doi.org/10.1242/dev.086223.

Kumar, M., P. Ray, and S. C. Chapman. 2012. "Fibroblast Growth Factor and Bone Morphogenetic Protein Signaling Are Required for Specifying Prechondrogenic Identity in Neural Crest-Derived Mesenchyme and Initiating the Chondrogenic Program." *Developmental Dynamics* 241, no. 6: 1091–1103. https://doi.org/10.1002/dvdy.23768.

LaMantia, A.-S., N. Bhasin, K. Rhodes, and J. Heemskerk. 2000. "Mesenchymal/Epithelial Induction Mediates Olfactory Pathway Formation." *Neuron* 28: 411–425.

Le Douarin, N. M., S. Creuzet, G. Couly, and E. Dupin. 2004. "Neural Crest Cell Plasticity and Its Limits." *Development* 131, no. 19: 4637–4650. https://doi.org/10.1242/dev.01350.

Lee, S.-H., K. K. Fu, J. N. Hui, and J. M. Richman. 2021. "Noggin and Retinoic Acid Transform the Identity of Avian Facial Prominences." *Nature* 414: 909–912.

Lee, C. A., C. Sánchez Moreno, and A. V. Badyaev. 2024. "FInCH: FIJI Plugin for Automated and Scalable Whole-Image Analysis of Protein Expression and Cell Morphology." *MethodsX* 13: 102855.

Lenne, P.-F., E. Munro, I. Heemskerk, et al. 2021. "Roadmap for the Multiscale Coupling of Biochemical and Mechanical Signals During Development." *Physical Biology* 18: 041501.

Li, Y., A. Li, J. Junge, and M. Bronner. 2017. "Planar Cell Polarity Signaling Coordinates Oriented Cell Division and Cell Rearrangement in Clonally Expanding Growth Plate Cartilage." *eLife* 6: e23279.

Lin, C. M., T. X. Jiang, R. B. Widelitz, and C. M. Chuong. 2006. "Molecular Signaling in Feather Morphogenesis." *Current Opinion in Cell Biology* 18, no. 6: 730–741.

Linde-Medina, M., B. Hallgrímsson, and R. Marcucio. 2016. "Beyond Cell Proliferation in Avian Facial Morphogenesis." *Developmental Dynamics* 245, no. 3: 190–196. https://doi.org/10.1002/dvdy.24374.

Liu, W., J. Selever, D. Murali, et al. 2005. "Threshold-Specific Requirements for Bmp4 in Mandibular Development." *Developmental Biology* 283, no. 2: 282–293. https://doi.org/10.1016/j.ydbio.2005.04.019.

Lu, J., B. Peng, W. Wang, and Y. Zou. 2024. "Epithelial-Mesenchymal Crosstalk: The Scriptwriter of Craniofacial Morphogenesis." *Frontiers in Cell and Developmental Biology* 12: 1497002. https://doi.org/10.3389/fcell.2024.1497002.

MacDonald, M. E., and B. K. Hall. 2001. "Altered Timing of the Extracellular-Matrix-Mediated Epithelial-Mesenchymal Interaction That Initiates Mandibular Skeletogenesis in Three Inbred Strains of Mice: Development, Heterochrony, and Evolutionary Change in Morphology." *Journal of Experimental Zoology* 291, no. 3: 258–273. https://doi.org/10.1002/jez.1102.abs.

Mallarino, R., O. Campàs, J. A. Fritz, et al. 2012. "Closely Related Bird Species Demonstrate Flexibility Between Beak Morphology and Underlying Developmental Programs." *Proceedings of the National Academy of Sciences of the United States of America* 109: 16222–16227.

Mallarino, R., P. R. Grant, B. R. Grant, A. Herrel, W. P. Kuo, and A. Abzhanov. 2011. "Two Developmental Modules Establish 3D Beak-Shape Variation in Darwin's Finches." *Proceedings of the National Academy of Sciences of the United States of America* 108: 4057–4062.

Medeiros, D. M., and J. G. Crump. 2012. "New Perspectives on Pharyngeal Dorsoventral Patterning in Development and Evolution of the Vertebrate Jaw." *Developmental Biology* 371, no. 2: 121–135. https://doi.org/10.1016/j.ydbio.2012.08.026.

Meinecke, L., P. P. Sharma, H. Du, L. Zhang, Q. Nie, and T. F. Schilling. 2018. "Modeling Craniofacial Development Reveals Spatiotemporal Constraints on Robust Patterning of the Mandibular Arch." *PLoS Computational Biology* 14, no. 11: e1006569. https://doi.org/10.1371/journal.pcbi.1006569.

Merrill, A. E., B. F. Eames, S. J. Weston, T. Heath, and R. A. Schneider. 2008. "Mesenchyme-Dependent BMP Signaling Directs the Timing of Mandibular Osteogenesis." *Development* 135, no. 7: 1223–1234. https://doi.org/10.1242/dev.015933.

Mina, M., Y. H. Wang, A. M. Ivanisevic, W. B. Upholt, and B. Rodgers. 2002. "Region- and Stage-Specific Effects of FGFs and BMPs in Chick Mandibular Morphogenesis." *Developmental Dynamics* 223, no. 3: 333–352. https://doi.org/10.1002/dvdy.10056.

Minoux, M., and F. M. Rijli. 2010. "Molecular Mechanisms of Cranial Neural Crest Cell Migration and Patterning in Craniofacial Development." *Development* 137, no. 16: 2605–2621. https://doi.org/10.1242/dev.040048.

Murray, J. R., C. W. Varian-Ramos, Z. S. Welch, and M. S. Saha. 2013. "Embryological Staging of the Zebra Finch, *Taeniopygia guttata*." *Journal of Morphology* 274, no. 10: 1090–1110. https://doi.org/10.1002/jmor.20165.

Noden, D. M. 1983. "The Role of the Neural Crest in Patterning of Avian Cranial Skeletal, Connective, and Muscle Tissues." *Developmental Biology* 96: 144–165.

Palmquist, K. H., S. F. Tiemann, F. L. Ezzeddine, et al. 2022. "Reciprocal Cell-ECM Dynamics Generate Supracellular Fluidity Underlying Spontaneous Follicle Patterning." *Cell* 185, no. 11: 1960–1973.e11. https://doi.org/10.1016/j.cell.2022.04.023.

Paudel, S., S. Gjorcheska, P. Bump, and L. Barske. 2022. "Patterning of Cartilaginous Condensations in the Developing Facial Skeleton." *Developmental Biology* 486: 44–55. https://doi.org/10.1016/j.ydbio.2022.03.010.

Potticary, A. L., E. S. Morrison, and A. V. Badyaev. 2020. "Turning Induced Plasticity Into Refined Adaptations During Range Expansion." *Nature Communications* 11: 3254.

Ransom, R. C., A. C. Carter, A. Salhotra, et al. 2018. "Mechanoresponsive Stem Cells Acquire Neural Crest Fate in Jaw Regeneration." *Nature* 563, no. 7732: 514–521. https://doi.org/10.1038/s41586-018-0650-9.

Ray, P., and S. C. Chapman. 2015. "Cytoskeletal Reorganization Drives Mesenchymal Condensation and Regulates Downstream Molecular Signaling." *PLoS One* 10, no. 8: e0134702. https://doi.org/10.1371/journal.pone.0134702.

Reid, B. S., H. Yang, V. S. Melvin, M. M. Taketo, and T. Williams. 2011. "Ectodermal WNT/β-Catenin Signaling Shapes the Mouse Face." *Developmental Biology* 349, no. 2: 261–269. https://doi.org/10.1016/j.ydbio.2010.11.012.

Richman, J. M., and C. Tickle. 1989. "Epithelia Are Interchangeable Between Facial Primordia of Chick Embryos and Morphogenesis Is Controlled by the Mesenchyme." *Developmental Biology* 136: 201–210.

Santagati, F., and F. M. Rijli. 2003. "Cranial Neural Crest and the Building of the Vertebrate Head." *Nature Reviews Neuroscience* 4, no. 10: 806–818. https://doi.org/10.1038/nrn1221.

Schneider, R. A. 2018. "Neural Crest and the Origin of Species-Specific Pattern." *Genesis* 56, no. 6–7: e23219. https://doi.org/10.1002/dvg.23219.

Schneider, R. A. 2024. "Cellular, Molecular, and Genetic Mechanisms of Avian Beak Development and Evolution." *Annual Review of Genetics* 58: 433–454. https://doi.org/10.1146/annurev-genet-111523-101929.

Schneider, R. A., and J. A. Helms. 2003. "The Cellular and Molecular Origins of Beak Morphology." *Science* 299: 565–568.

Selleri, L., and F. M. Rijli. 2023. "Shaping Faces: Genetic and Epigenetic Control of Craniofacial Morphogenesis." *Nature Reviews Genetics* 24, no. 9: 610–626. https://doi.org/10.1038/s41576-023-00594-w.

Shahbazi, M. N., A. Scialdone, N. Skorupska, et al. 2017. "Pluripotent State Transitions Coordinate Morphogenesis in Mouse and Human Embryos." *Nature* 552, no. 7684: 239–243. https://doi.org/10.1038/nature24675.

Shyer, A. E., A. R. Rodrigues, G. G. Schroeder, E. Kassianidou, S. Kumar, and R. M. Harland. 2017. "Emergent Cellular Self-Organization and Mechanosensation Initiate Follicle Pattern in the Avian Skin." *Science* 357, no. 6353: 811–815. https://doi.org/10.1126/science.aai7868.

Soldatov, R., M. Kaucka, M. E. Kastriti, et al. 2019. "Spatiotemporal Structure of Cell Fate Decisions in Murine Neural Crest." *Science* 364, no. 6444: eaas9536. https://doi.org/10.1126/science.aas9536.

Svandova, E., R. Peterkova, E. Matalova, and H. Lesot. 2020. "Formation and Developmental Specification of the Odontogenic and Osteogenic Mesenchymes." *Frontiers in Cell and Developmental Biology* 8: 640. https://doi.org/10.3389/fcell.2020.00640.

Tacchetti, C., S. Tavella, B. Dozin, R. Quarto, G. Robino, and R. Cancedda. 1992. "Cell Condensation in Chondrogenic Differentiation." *Experimental Cell Research* 200: 26–33.

Tak, H. J., T. J. Park, Z. Piao, and S. H. Lee. 2017. "Separate Development of the Maxilla and Mandible Is Controlled by Regional Signaling of the Maxillomandibular Junction During Avian Development." *Developmental Dynamics* 246, no. 1: 28–40. https://doi.org/10.1002/dvdy.24465.

Trainor, P. A., L. Ariza-McNaughton, and R. Krumlauf. 2002. "Role of the Isthmus and FGFs in Resolving the Paradox of Neural Crest Plasticity and Prepatterning." *Science* 295: 1288–1291.

Van Otterloo, E., I. Milanda, H. Pike, et al. 2022. "AP-2α and AP-2β Cooperatively Function in the Craniofacial Surface Ectoderm to Regulate Chromatin and Gene Expression Dynamics During Facial Development." *eLife* 11: e70511. https://doi.org/10.7554/eLife.70511.

Welsh, I. C., and T. P. O'Brien. 2009. "Signaling Integration in the Rugae Growth Zone Directs Sequential SHH Signaling Center Formation During the Rostral Outgrowth of the Palate." *Developmental Biology* 336, no. 1: 53–67. https://doi.org/10.1016/j.ydbio.2009.09.028.

Widelitz, R. B., T. X. Jiang, B. A. Murray, and C. M. Chuong. 1993. "Adhesion Molecules in Skeletogenesis: II. Neural Cell Adhesion Molecules Mediate Precartilaginous Mesenchymal Condensations and Enhance Chondrogenesis." *Journal of Cellular Physiology* 156, no. 2: 399–411. https://doi.org/10.1002/jcp.1041560224.

Wood, B. M., V. Baena, H. Huang, D. M. Jorgens, M. Terasaki, and T. B. Kornberg. 2021. "Cytonemes With Complex Geometries and Composition Extend Into Invaginations of Target Cells." *Journal of Cell Biology* 220, no. 5: e202101116. https://doi.org/10.1083/jcb.202101116.

Woronowicz, K. C., and R. A. Schneider. 2019. "Molecular and Cellular Mechanisms Underlying the Evolution of Form and Function in the Amniote Jaw." *EvoDevo* 10: 17. https://doi.org/10.1186/s13227-019-0131-8.

Wu, P., T. X. Jiang, J.-Y. Shen, R. B. Widelitz, and C. M. Chuong. 2006. "Morphoregulation of Avian Beaks: Comparative Mapping of Growth Zone Activities and Morphological Evolution." *Developmental Dynamics* 235: 1400–1412.

Wu, P., T. X. Jiang, S. Suksaweang, R. B. Widelitz, and C. M. Chuong. 2004. "Molecular Shaping of the Beak." *Science* 305: 1465–1466.

Xavier, G. M., M. Seppala, W. Barrell, A. A. Birjandi, F. Geoghegan, and M. T. Cobourne. 2016. "Hedgehog Receptor Function During Craniofacial Development." *Developmental Biology* 415, no. 2: 198–215. https://doi.org/10.1016/j.ydbio.2016.02.009.

Xu, J., P. P. R. Iyyanar, Y. Lan, and R. Jiang. 2023. "Sonic Hedgehog Signaling in Craniofacial Development." *Differentiation* 133: 60–76. https://doi.org/10.1016/j.diff.2023.07.002.

Yamaguchi, T. P., A. Bradley, A. P. McMahon, and S. Jones. 1999. "A Wnt5a Pathway Underlies Outgrowth of Multiple Structures in the Vertebrate Embryo." *Development* 126: 1211–1223.

Yoon, B. S., R. Pogue, D. A. Ovchinnikov, et al. 2006. "BMPs Regulate Multiple Aspects of Growth-Plate Chondrogenesis Through Opposing Actions on FGF Pathways." *Development* 133, no. 23: 4667–4678. https://doi.org/10.1242/dev.02680.

Zheng, C., Y. Hu, M. Sakurai, et al. 2021. "Cell Competition Constitutes a Barrier for Interspecies Chimerism." *Nature* 592: 272–276. https://doi.org/10.1038/s41586-021-03273-0.

Supporting Information

Additional supporting information can be found online in the Supporting Information section.
Supporting File: ede70044-sup-0001-SupplementaryMaterials.pdf.